

Shear and breathing modes of layered materials

Giovanni Pizzi,^{1,*} Silvia Milana,² Andrea C. Ferrari,² Nicola Marzari,¹ and Marco Gibertini^{1,3,4,†}

¹*Theory and Simulation of Materials (THEOS), and National Centre for Computational Design and Discovery of Novel Materials (MARVEL),*

École Polytechnique Fédérale de Lausanne, CH-1015 Lausanne, Switzerland

²*Cambridge Graphene Centre, University of Cambridge, Cambridge CB3 0FA, UK*

³*Department of Quantum Matter Physics, University of Geneva, CH-1211 Genève, Switzerland*

⁴*Dipartimento di Scienze Fisiche, Informatiche e Matematiche, University of Modena and Reggio Emilia, IT-41125 Modena, Italy*

Layered materials (LMs), such as graphite, hexagonal boron nitride, and transition-metal dichalcogenides, are at the centre of an ever increasing research effort, due to their scientific and technological relevance. Raman and infrared spectroscopies are accurate, non-destructive, approaches to determine a wide range of properties, including the number of layers and the strength of the interlayer interactions. Here, we present a general approach to predict the complete spectroscopic fan diagrams, i.e., the relations between frequencies and number of layers, N , for the optically-active shear and layer-breathing modes of any multilayer comprising $N \geq 2$ identical layers. In order to achieve this, we combine a description of the normal modes in terms of a one-dimensional mechanical model, with symmetry arguments that describe the evolution of the point group as a function of N . Group theory is then used to identify which modes are Raman and/or infrared active, and to provide diagrams of the optically-active modes for any stack composed of identical layers. We implement the method and algorithms in an open-source tool directly available on the Materials Cloud portal, to assist any researcher in the prediction and interpretation of such diagrams. Our work will underpin all future efforts on Raman and Infrared characterization of known, and yet not investigated, LMs.

I. INTRODUCTION

Layered materials (LMs) are at the centre of an ever growing research effort due to the variety of their potential applications in a wide range of fields[1]. There are at least 5000 materials that are layered[2] with at least 1800 that are readily exfoliable[2–5], and even more that could be synthesised[6–9]. However, only a very small fraction of these have been experimentally investigated to date, such as graphene, hexagonal boron nitride (hBN), black phosphorous (BP), transition metal dichalcogenides (TMDs), InSe and other monochalcogenides, MAXenes, and very few others. When a given LM is exfoliated into a multilayer (ML), the optical and electronic properties change with the number of layers (N). For a given N , the properties can be tuned by varying the relative orientation of the layers[10–13]. For a given N and orientation, properties can also be changed by arranging different LMs together in heterostructures (LMHs)[14–19]. The degrees of freedom are such that it will take decades, if ever, before all possible LMs will be exfoliated and investigated when arranged in LMHs, as a function of N and of relative orientation. Due to the extraordinary range of properties that can be addressed, it is essential to develop approaches to readily identify N in any given assembly or device.

Techniques to measure N in a given sample based on optical contrast[20] have been developed. However, they

depend on the substrate and do not readily provide information such as strain or doping. A more informative approach is offered by Raman[21] and infrared (IR)[22] spectroscopies that probe phonons in a given material.

In particular, in LMs there are two fundamentally different sets of modes. Those coming from the relative motion of the constituent atoms within each layer, usually found at high frequencies ($>100 \text{ cm}^{-1}$)[21], and those due to relative motions of the layers themselves, either perpendicular, C modes, or parallel, layer breathing (LB) modes, to their normal[21, 23–25]. Several studies have identified these modes in a limited set of ML-LMs, like ML-graphene[26–29], TMDs (such as MoS₂[30, 31], MoSe₂[32], WS₂[33], WSe₂[34], MoTe₂[35, 36], ReS₂[37–39], PtS₂[40]), NbSe₂[41–43], hBN[44], phosphorene[45–47], Bi₂X₃[48], and metal chalcogenides (like GaSe[49, 50], InSe[50], and SnS₂[51]).

The optically-active (Raman or IR) modes can be plotted as a function of N , in a graph that represents a fan, and it is thus called a fan diagram[26]. The experimental data can be explained with a linear chain model[26], whereby each plane is linked to the next one by a spring, modelled by scalar interlayer force constants corresponding to a motion parallel (C) or perpendicular (LB) to the planes[26].

Here, we extend the linear chain model to every possible exfoliable LM composed of identical layers by implementing a group-theory approach. This starts from the bulk LM symmetry properties to derive a general tensorial expression for the interlayer force constants. We show how to derive the evolution of the point group for any N of a ML, knowing the space group of the bulk structure, considered as the repetition of a single layer

* giovanni.pizzi@epfl.ch

† marco.gibertini@unimore.it

stacked recursively. This is then used to assign each normal mode to a given irreducible representation of the corresponding point group, in order to assess its optical activity and obtain the fan diagram of each LM. Finally, we provide an online tool, available on the Materials Cloud[52] at the address <https://materialscloud.org/work/tools/layer-raman-ir>, that accepts user-supplied structures and computes on the fly the corresponding fan diagram and symmetry-compliant form of the interlayer force constants. Our work provides the interpretation of the patterns that are measured in experimental fan diagrams of any LM composed of identical layers, either already experimentally investigated, or, more importantly, any of the thousands that will be studied in the future.

II. FAN DIAGRAMS: PREDICTION AND INTERPRETATION

A fan diagram is a plot of the normal-mode frequencies associated with the rigid relative motion of the layers in a ML-LM, as a function of N . The fan diagram frequencies are a fingerprint of each material. Their trend as a function of N depends on the atomic structure and on the symmetry both of ML-LM system and of the corresponding bulk LM.

We now develop a theoretical model to interpret the experimental results and assess the origin and character of these vibrational modes and their expected optical activity. Such a model needs a number of components.

1. We need an approach to compute the normal vibrational modes of ML-LMs and their frequencies, using a model that can capture the system geometry, and only depends on a few material parameters, such as the elastic constants between each pair of layers.
2. We need to numerically identify and extract the layers of a ML-LMs from the bulk structure and analyse their crystal symmetry. Given the space group of bulk LMs, it is possible to determine all possible symmetries of ML-LMs system with a given N .
3. We need to exploit the symmetry information to identify the optical activity of each normal mode (i.e., if the mode is Raman or IR active, and, if so, if it can be detected in the most commonly used back-scattering geometry[21, 53]). We achieve this by using group theory to classify each mode, assigning it to the irreducible representation to which it belongs, thus determining its optical activity.
4. We then combine points 1-3 above in a single model to enable the interpretation of the experimental data.

This paper is organised such that a reader interested only in the applications of this method can skip the rest of this Sec. II and move directly to the results reported in Sec. III and to the description of the free online tool, presented in Sec. IV, that applies this approach to any user-provided LM.

A. Definition of a layered material and nomenclature

We are interested in modelling the vibrational properties of LMs when layers move essentially as rigid units as a consequence of the strong covalent bonds between atoms in a given layer, as opposed to the weak van-der-Waals interactions keeping layers together.

In this limit, vibrations can be described in terms of interlayer force constants, acting as restoring forces between nearby layers.

In order to limit the number of parameters in the model and make use of crystal symmetry and space-group concepts to seamlessly predict the normal modes and their optical activity, we consider LMs with a sufficiently regular stacking (to be described below, in particular focusing on LMs composed of identical layers), which covers the majority of naturally occurring LMs.

In this paper we cover any multilayer comprising $N \geq 2$ identical layers. We note that our approach can be numerically extended to any LM and LMH. Stacking in LMHs lowers the symmetry, lifting most symmetry constraints on the optical activity of modes. Group theory alone could predict modes to be active even if the corresponding intensity might be negligible; thus further computation of the optical-coupling matrix elements becomes essential. In non-recursive stacking sequences, more parameters enter the description of interlayer force constants (with a different force-constant matrix for each layer pair and for each possible relative orientation of the two), which can be extracted from additional first-principles simulations.

We follow a practical approach, giving a brief and intuitive explanation of the important symmetry properties of these LMs. Ref. 54 provides a complete treatment with formal definitions and proofs. Since the nomenclature used in the experimental literature of ML fan diagrams often differs from that used in the crystallographic community[54], we also provide a mapping between the names used in the two communities, where appropriate.

ML-LMs are called polytypes by the International Union of Crystallography (see Ref. 55 for a formal definition). A theory to describe these ML-LMs, based solely on the symmetry of each layer and on the symmetry relation between subsequent layers, was developed in Refs. 56 and 57.

We limit our study to LMs where all layers are identical and can be mapped onto each other through coincidence operations, defined as isometries (i.e., space transformations that preserve the distance between any two points)

bringing a layer of the ML-LM onto the next one. As already noted above this excludes, e.g., bulk LMHs formed by different LMs, as in the case of franckeite[58, 59] but is the typical case for exfoliable materials.

The coincidence operation that brings one layer onto the next might not be the same for all layers, e.g., if the first layer is mapped onto the second one by a translation, while the second is mapped onto the third by a rotation. Again with the goal to limit the number of parameters in the model, we then consider an additional requirement by limiting our analysis to MDO (maximum degree of order) polytypes. These are LMs where the coincidence operation is total, i.e., it is the same between any pair of adjacent layers. As a consequence[54], in a MDO polytype any triplet of subsequent layers is equivalent, while it is not true that every pair is equivalent, as we shown in the example of Fig. 1c for Bi_2TeI . As any triplet is equivalent, MDO polytypes have only 1 or 2 independent interatomic force-constant tensors that occur between nearby layers in the triplet, while all other tensors can be reconstructed using symmetry arguments. If the coincidence operation is not total, the relative arrangement of atoms in pairs of subsequent layers could be very different, leading to different interactions between them, even if this almost never occurs in naturally occurring exfoliable materials.

Within these constraints, we can classify all LMs in 3 categories[54], shown with 3 examples in Fig. 1.

We first consider the case where each layer is non-polar along the stacking direction (i.e., it has a symmetry that flips it upside down) and then when it is polar. In the non-polar case, only one possibility exists (Category I, Fig. 1a). In the polar case there are 2 options: either the polarity has the same orientation for all layers (Category II, Fig. 1b) or it alternates between layers (Category III, Fig. 1c). These three categories have very different sets of symmetry operations. We note that Category III, while considered here for completeness from a symmetry point of view, never occurs to the best of our knowledge for the most common LMs, such as graphite, hBN or the TMDs.

We define the planes of the layers in the LM as the “horizontal” direction, and the stacking direction of the LM as the “vertical” or z one (note that the third vector of the bulk unit cell might not be orthogonal to the plane of the layers, see, e.g., Fig. 1c).

We then distinguish the symmetry operations of the 1L-LM (called λ symmetries in Ref. 54) and the coincidence operations bringing a layer onto the next one (σ symmetries).

Any symmetry operation can either change the sign of any vertical coordinate, i.e., flip the layer upside down (called ρ operations[54], like inversion, roto-reflections, reflections under horizontal planes, or two-fold rotations with an horizontal axis) or not change the sign of vertical-direction coordinates (called τ operations[54], e.g., translations, rotations with a vertical axis, or reflections under vertical planes; these form a subgroup). Since, in a LM, all ρ operations change the stacking order of the layers (e.g., a stacking 1-2-3-1-2-3 becomes 3-2-1-3-2-1), in

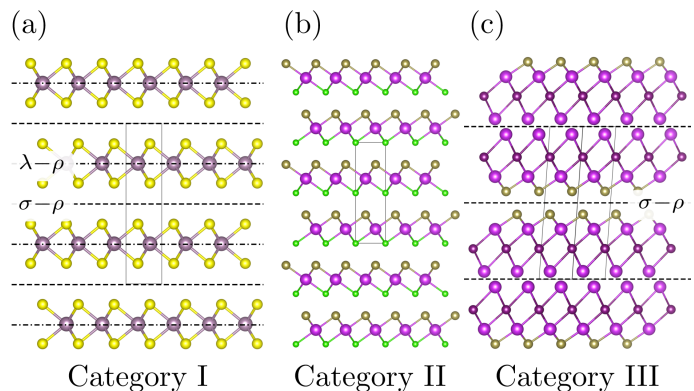


FIG. 1. 3 categories of LMs allowed from a symmetry point of view, for MDO polytypes of equivalent layers. (a) Category I: each layer is non-polar along the stacking direction (i.e., it has a symmetry operation that flips it upside down), such as in MoS_2 (structure from the Crystallography Open Database (COD[60]), code 9007660). Mo atoms are shown in violet and S atoms in yellow. (b) Category II: each layer is polar along the stacking direction, and all layers are oriented in the same direction, such as in BiTeCl (structure from the Inorganic Crystal Structure Database (ICSD[61]), code 79362). Bi atoms are shown in light purple, Te atoms in brown, and Cl atoms in green. (c) Category III: each layer is polar along the stacking direction, and they stack in alternating polarisation directions, such as Bi_2TeI (ICSD[61] code 153858). Bi atoms are shown in light purple, Te atoms in brown, and I atoms in dark purple. Symmetry planes for layer-order-changing operations (ρ planes) are indicated with dashed lines (σ operations) or dotted-dashed lines (λ operations). Note that the LM in Category III is for illustrative purposes: depending on the nature chemical bonding, this could be considered as 3 non-equivalent layers (2 BiTeI layers analogous to those of Category II, and one layer of Bi atoms)

the following we call them layer-order-changing (LOC) operations[62], while we call the τ ones non-LOC operations.

With these definitions, for non-polar layers (Fig. 1a) both λ and σ operations can be either LOC or non-LOC[54]. Thus, we can formally define the vertical z coordinate of each layer as the z coordinate of its inversion centre (or reflection plane or rotation axis). The plane with this z coordinate is called the layer plane[54]. Then, LOC operations can either be λ , and in this case their symmetry elements are on a layer plane, or σ , and they must lie on planes halfway between layer planes, as shown in Fig. 1a. We will call these planes “middle planes”. Non-LOC σ operations (bringing one layer onto the next) are always combined with a translation along the vertical direction.

Polar layers do not have any symmetry operation that flips the z coordinates, so all λ operations are non-LOC. However, while in Category II of Fig. 1 also all σ coincidence operations are non-LOC (because the polarity direction is never reversed), in Category III all σ coincidence operations must be LOC (changing thus polar-

TABLE I. Summary table of the type of operations in each of the categories of Fig. 1.

Category	Polar layers	λ (operations of the monolayer)		σ (operations bringing a layer onto the next one)	
		$\lambda - \rho$ (λ LOC)	$\lambda - \tau$ (λ non-LOC)	$\sigma - \rho$ (σ LOC)	$\sigma - \tau$ (σ non-LOC)
I	✗	✓ (on layer plane)	✓	✓ (on middle plane)	✓
II	✓	✗	✓	✗	✓
III	✓	✗	✓	✓ (on middle plane)	✓

sation orientation between consecutive layers) and they also lie on middle planes. In Category III we cannot univocally define a layer plane, since there is no layer inversion plane, but by symmetry it is instead possible to define two sets of middle planes.

This distinction into 3 Categories is very important for the modelling of the interlayer force constants. In Categories I, II, all pairs of layers are equivalent, therefore the same interlayer force constant matrix can be used to describe the interaction between any pair of layers. In Category III there are 2 different interlayer force constant matrices, depending on whether the polarisations of the two neighbouring layers are pointing inwards or outwards with respect to the van-der-Waals gap between them (see more detailed discussions in Sec. II C and Appendix C).

When a LM satisfies all the conditions above the description of its vibrational properties and of the symmetries of ML-LM is greatly simplified and can be carried out analytically or semi-analytically. For this reason in the rest of the paper we focus only on this class of LMs. Nonetheless, our approach can be seamlessly extended to any form of LMs or even LMHs, although a numerical treatment might in general be needed, with a decreased predictivity owing to the increased number of free parameters.

B. Obtaining the point group of a ML-LM

We now consider how to obtain the point group of a ML-LM with N layers (needed to predict its optical activity) given the point group of its parent bulk LM (B-LM), i.e., extended periodically in the direction orthogonal to the layers.

We call n_c the number of layers in the B-LM conventional cell, and n_p the number of layers in the B-LM primitive cell. These two numbers are in general different, e.g., for centred cells or for rhombohedral systems. For instance, rhombohedral graphite has $n_c = 3$ and $n_p = 1$. We also define the “stacking index” of a layer as an integer indexing the layers so that, e.g., if a layer has stacking index ℓ , then the next layer (in the positive vertical direction) has stacking index $\ell + 1$.

The stacking direction, orthogonal to the planes of the layers, is unique. Thus for some crystal systems it is prescribed by symmetry. In particular, in tetragonal, hexagonal and trigonal systems, the stacking direction must be along the n -fold characteristic symmetry axis

(e.g., the c axis for tetragonal systems): if this was not the case, the n -fold rotations (with $n > 2$) would bring the stacking direction into other distinct staking directions, which violates its unicity. The same arguments imply that cubic systems are not compatible with a layered structure[62, 63]: if a given direction, say z , were the stacking direction, then also x and y should be by symmetry, as in cubic systems all principal directions are equivalent. Therefore, we do not consider cubic systems in the rest of this work.

In orthorhombic, monoclinic and triclinic systems the stacking direction is instead not prescribed by symmetry, therefore the space group alone is not sufficient to characterise the system. Instead, we need to consider all inequivalent settings, i.e., possible non-conventional choices for the origin and lattice vectors with respect to symmetry elements. We consider all settings that are typically discussed in crystallography[64, 65], identified by their Hall number[66]. This ranges from 1 to 488 if we exclude cubic systems. E.g., space group 17 (P222₁, a primitive orthorhombic system with one screw axis and no mirror symmetry) can be realised in three different settings, depending on the direction of the screw axis, with Hall number 109, 110, and 111 for the screw axis aligned along the third, first and second cell axis, respectively. In this work we are always assuming the stacking direction to be orthogonal to the first two lattice vectors. Then, for setting P222₁ with Hall number 109, the 2₁ screw axis is along the stacking direction, and a ML in this Hall setting has different symmetry properties than Hall numbers 110 and 111, corresponding to P2₁22 and P22₁2, that are equivalent for our purposes because in both cases the screw axis is horizontal.

We now present a strategy to obtain “compatibility relations”, i.e., rules determining the possible point groups G_N of a ML-LM as a function of N , by knowing the B-LM space group and setting (thus also the B-LM point group G_b), and the direction along which the material is layered. This allows us to identify which point-group operations of the B-LM (i.e., of G_b) are part of G_N .

We consider $N \geq n_p$. In this case, G_N is a subgroup of G_b because any operation of the ML-LM must also be an operation of the B-LM for a MDO polytype. For $N < n_p$, this is not always true as we discuss in Appendix D, and so this case requires an independent treatment. We note that n_p is either 1 or 2 for the most studied LMs, such as black phosphorous and rhombohedral graphite ($n_p = 1$) or MoS₂, hBN, and Bernal-stacked graphite ($n_p = 2$).

Since the modes plotted in the fan diagrams (i.e., relative rigid oscillations of the layers) only exist for $N \geq 2$, the condition $N \geq n_p$ is thus not a strong limitation.

We first consider non-LOC operations. Non-LOC σ operations ($\sigma - \tau$) can never be symmetries of a finite ML-LM, because they map each layer with stacking index ℓ onto the layer with stacking index $\ell + 1$. For λ non-LOC ($\lambda - \tau$) symmetries, these non-LOC layer-invariant operations form a group[62] that we call the layer-invariant point group, G_I , which is a subgroup of G_b . Since all elements of G_I leave each layer invariant individually (i.e., they map each layer onto itself[62]), they are also symmetry operations of the ML for any N . Thus, G_I is a subgroup of G_N . Given a B-LM space group, obtaining G_I amounts to considering all B-LM symmetry operations that are non-LOC, take only their rotational part, and check which point group they form. G_I for all space groups and settings is in Table III.

To obtain the complete G_N , we have to complement G_I with all LOC (ρ) operations of the ML-LM, which are a subset of the LOC operations of the B-LM. For Category II, no LOC operations exist in B-LM, see Table I. Therefore, there are no additional operations to consider and $G_N = G_I$, independently of N and n_c . For Categories I and III, LOC operations exist, and we need to select the B-LM LOC operations compatible with a finite ML-LM.

We focus our attention on Category I because, as explained in Appendix C, Category III can be considered as a special case of Category I for the determination of the point group. For a ML-LM with N layers, if an inversion centre for a LOC operation exists, this must be the layer plane of the central layer if N is odd (e.g., layer with stacking index 3 if $N = 5$), or the middle plane between the two central layer planes if N is even. Therefore, the ML-LM point group G_N will be obtained complementing G_I with only those LOC operations that have inversion planes respectively on a layer plane or on a middle plane.

For Category I there is always at least one operation with such a plane. As explained in Appendix B, if n_c is odd, any LOC can be both considered as having a symmetry on a layer plane or (with a different fractional translation) on a middle plane, so all of them can be included when computing G_N . Instead, for even n_c (see Appendix B), LOCs can either have inversion on a layer plane, or on a middle plane. Depending on the parity of N , two point groups might alternate, corresponding to which set of LOCs is compatible with N .

Table III reports the complete set of possible ML-LM point groups G_N for each Hall setting and for $n_c = 1, \dots, 6$. Table III often gives 2 symbols (\surd or \times) instead of one or two possible point groups G_N . These indicate cases in which it is impossible to create a ML in that setting and with the specified n_c in the conventional cell. The meaning of the two symbols is explained in the Table caption and, in detail, in Appendix B.

We now illustrate with a few examples how to use Table III (noting that the online tool presented in Sec. IV

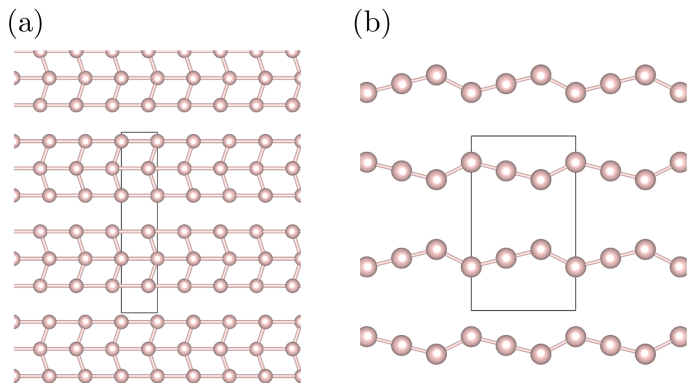


FIG. 2. Two fictitious crystals with same B-LM space group (51, Hall number 242, Hall symbol $P2/c2/m2_1/m$) and $n_c = 2$ (with an orthorhombic unit cell and translational invariance in the y direction orthogonal to the page). (a) 1L has mirror symmetry but no inversion. The alternation of point groups for ML is $2/m$ for even N , $mm2$ for odd N . (b) 1L has inversion symmetry but no mirror plane. The alternation of point groups for ML is $mm2$ for even N , $2/m$ for odd N .

performs the symmetry analysis automatically without the need to check the table).

Given a LM, we first need to identify its layers, and determine in which category of Fig. 1 the materials falls in, depending on the symmetry of the 1L-LM.

Let us start with an example for Category I. If we consider MoS_2 (in its 2H phase), hBN, or Bernal graphite, in all these cases the 1L-LM is non-polar (there is a symmetry operation that flips it upside down), so they belong to Category I, and the bulk space group is $P6_3/m2/m2/c$ (194), with a single choice of Hall number (488). $n_c = 2$ in all these cases (see, e.g., Fig. 1a). Then, Table III shows that the possible ML-LM point groups are $\bar{6}m2$ and $\bar{3}m$. $\bar{6}m2$ is for odd N (which does not have a centre of symmetry) while $\bar{3}m$ occurs for even N ($\bar{3}m$ has a centre of symmetry). We emphasise here again the assumption $N \geq n_c$. For graphene ($N = 1$) the point group is $6/mmm$, i.e., neither of the two point groups occurring for $N \geq 2$ (for the reasons explained in Appendix D). This can be understood considering that graphene has an additional centre of symmetry, that disappears in the graphite stacking for any odd $N > 1$.

From our analysis it is only possible to identify the set of possible G_N given the Hall number and n_c . To make a specific assignment for odd and even N , as in the above example, it is necessary to know the 1L symmetries. To illustrate this, Figs. 2a,b show two fictitious crystals with the same B-LM space group (51, Hall number 242, Hall symbol $P2/c2/m2_1/m$) and $n_c = 2$. From Table III the 2 possibilities for G_N are i) $2/m$ (having inversion) or ii) $mm2$ (not having inversion). In both cases the B-LM has both inversion symmetry and horizontal mirror symmetry, with a corresponding B-LM point group $G_b = mmm$. However, 1Ls have either horizontal reflection symmetry only (Fig. 2a) or inversion symmetry only (Fig. 2b). As

a result, the inversion and mirror LOC operations have different centres in B-LMs, with the inversion centre on middle (layer) planes for Fig. 2a (Fig. 2b), and horizontal mirror symmetry on layer (middle) planes for Fig. 2a (Fig. 2b). Since symmetries from middle planes are selected for even N and those from layer planes for odd N , for Fig. 2a the assignment is $2/m$ for even N and $mm2$ for odd N . The opposite holds for Fig. 2b.

We now consider some examples from Categories II, III. BiTeCl (Fig. 1b) has B-LM space group $P6_3mc$ (186, Hall number 480). Since each layer is polar, and all layers have the same polarity (Category II), the point group of any ML-BiTeCl will be $G_I = 3m$ (see Table III) as explained in Appendix B. For Bi₂TeI (Fig. 1c), instead, the B-LM space group is $C2/m$ (12, Hall number 63). Since it belongs to Category III, the point group of any ML-Bi₂TeI with odd N will be $G_I = m$. If instead N is even, then we need to check in Table III the column for $n_c = 1$ (as explained in Appendix C: Table III can be used but interpreting n_c in the table as the number of layer pairs, i.e., half of the number of layers in the bulk conventional cell), so that the resulting point group is $2/m$, independent of the termination of the ML-Bi₂TeI. Since, as we discussed earlier, some entries in Table III have two possible values, this implies that for some space groups we might have an alternation of point groups G_N for N multiple of 4 or multiple of 2 only, and the specific point group taken will depend on the termination of the finite ML.

C. Computing normal modes

In a fan diagram, we focus only on vibrational modes associated with a rigid relative motion of the layers, that are typically those with lower energy $< 100 \text{ cm}^{-1}$.

The simplest approximation[26] is to model the ML-LM as a finite linear chain model of masses with a force constant K between them, which might depend on the direction of motion. This model is often able to capture the qualitative behaviour of the frequency of the modes as a function of N , but it might not be able to predict accurately the frequencies or the coupling between C and LB modes in some systems. Extensions of this model have been proposed to include further neighbours[29] or intralayer coupling[67], e.g., in the case of MoS₂, where a diatomic chain model has been derived[30] to take into account the two types of atoms in the system (Mo and S).

Since layers are held together by van-der-Waals forces (typically much weaker than the chemical bonds between atoms in a layer), in the following we derive a more general tensorial model under the following two assumptions: 1) layers move as rigid units, i.e., the atomic displacements $\mathbf{u}(\ell)$ depend only on the stacking index ℓ ; 2) we include only first neighbour interactions between layers. These two assumptions are typically very good in most ML-LMs[23–25]. Thus, even when they break, such as at

the interface between twisted graphene multilayers[29], the predictions of our model are still useful to qualitatively interpret experimental data.

Under these assumptions, the equation of motion can be then written as:

$$M\ddot{u}_\alpha(\ell) = \sum_\beta \left\{ K_{\alpha\beta}^{(\ell)} [u_\beta(\ell+1) - u_\beta(\ell)] + K_{\alpha\beta}^{(\ell-1)} [u_\beta(\ell-1) - u_\beta(\ell)] \right\}, \quad (1)$$

where M is the 1L total mass per unit cell, α and β are Cartesian directions, and $K_{\alpha\beta}^{(\ell)}$ is the (tensorial) force constant between layer ℓ and $(\ell+1)$. Eq. (1) is valid for B-LMs when periodic boundary conditions are applied, $u_\beta(\ell = n_c + 1) = u_\beta(\ell = 1)$, and for finite ML-LMs when all $u_\beta(\ell)$ terms for $\ell < 0$ or $\ell > N$ are removed.

The $K_{\alpha\beta}^{(\ell)}$ tensor, describing the interaction between two adjacent layers, can be different for each pair of layers. For Category III of Fig. 1, there are two types of interfaces that alternate: one set having Te atoms facing each other, the other having Bi atoms, and the corresponding force constants will thus be different. Even for Categories I, II, where all layers and layer interfaces are identical, the matrices for different interfaces between layers ℓ and $\ell+1$ can differ, e.g., because an interface is obtained from the previous one by a rotation along the vertical axis, or some other symmetry operation (e.g., as for MoS₂ and BiTeCl, see Fig. 1a,b). In these cases, the matrices are related between them by the coincidence operation bringing one layer onto the next one, and we can write $K^{(\ell+1)} = RK^{(\ell)}R^{-1} = R^{\ell-1}KR^{-\ell+1}$, with R being the rotational part of the coincidence operation, and $K = K^{(1)}$ the interlayer force constant between the first and the second layer of the stack. For Category III, $K^{(\ell)}$ can be generated in an analogous way starting from one of the two matrices $K^{(1)}$ and $K^{(2)}$, depending on the parity of ℓ . We thus expect in general not a single $K_{\alpha\beta}^{(\ell)}$, but a set of interlayer force-constant matrices, depending on a few parameters.

In the online tool described in Sec. IV we apply and solve numerically Eq. (1), and so we use the appropriately transformed $K^{(\ell)}$ for each layer. However, in order to get a qualitative understanding of the frequencies, their degeneracies, and their interpretation as C or LB modes, we summarise here the analytical results when there is a single $K_{\alpha\beta}$ for all layer pairs (i.e., we are in Categories I or II, and the operation R commutes with $K_{\alpha\beta}^{(1)}$, so that all K matrices turn out to be identical). This is the case, for instance, of MoS₂ or hBN.

Since $K_{\alpha\beta}$ is symmetrical, it can be diagonalised with eigenvalues k_1 , k_2 and k_3 . Then, one can solve the equation of motion to obtain $3N$ solutions (for a ML with N layers) obtaining[26, 34]:

$$u_\beta^{(\nu,n)}(\ell, t) = V_{\beta\nu} \cos \left[\frac{(n-1)(2\ell-1)\pi}{2N} \right] e^{i\omega^{(\nu,n)}t}, \quad (2)$$

where $V_{\beta\nu}$ are the eigenvectors of $K_{\alpha\beta}$ and $\nu = 1, 2, 3$ denotes 3 branches (of N modes each, indexed by $n = 1, \dots, N$). The corresponding vibrational frequencies are given by:

$$\begin{aligned}\omega^{(\nu,n)} &= \sqrt{\frac{2k_\nu}{M} \left[1 - \cos\left(\frac{(n-1)\pi}{N}\right) \right]} = \\ &= 2\sqrt{\frac{k_\nu}{M}} \sin\left(\frac{(n-1)\pi}{2N}\right).\end{aligned}\quad (3)$$

The oscillation direction in each branch ν coincides with one of the principal directions of the symmetric tensor, identified by the eigenvector $V_{\beta\nu}$. In order to define C and LB modes, corresponding respectively to oscillations parallel to the layers (in the xy plane) and out-of-plane (along z), the K matrix must be block-diagonal, with a 2×2 block for the C modes and a 1×1 element for the LB block. In this case, we can then define if ν is a C or LB mode. We note that the frequency of the highest C mode in a ML with N layers is also called $\text{Pos(C)}_N = \frac{\omega^{(C,N)}}{2\pi c} = \frac{1}{\pi c} \sqrt{\frac{k_\nu}{M}} \cos\left(\frac{\pi}{2N}\right)$, when expressed as a wavelength (with c being the speed of light) and similarly Pos(LB)_M refers to the highest LB mode.

In general, however, the K matrix does not have such block form, and then the in-plane and out-of-plane vibrations are not decoupled, meaning that a distinction between LB and C modes is not possible, e.g., in the case of WTe_2 (see also Appendix E for an in-depth discussion on the separation of C and LB modes depending on the symmetry).

Since K describes the interaction between adjacent layers, its tensorial form (which elements are zero, which elements are equal to each other) depends on the crystal system [68] of the 2L-LM obtained by isolating the two layers, which is directly obtained from its point group.

All 7 possible cases [68] (skipping cubic systems that, as discussed in Sec. II B, are not compatible with a layered structure) are reported in Table II. For 2L-LMs, we have that for trigonal, hexagonal, and tetragonal systems a distinction between LB and C modes is possible and the C branches are degenerate. For orthorhombic systems, LB and C modes can be still defined, but the degeneracy of the two C branches is now lifted. For monoclinic systems, we can distinguish 2 cases: (i) in-plane monoclinic unique axis, for which we can identify one pure C branch, while the other two branches are mixed (no pure LB mode can be defined, e.g., WTe_2); (ii) unique axis along the stacking direction, for which we can distinguish LB and C modes, even though the C polarisation has no specific orientation with respect to the crystal axes. For triclinic systems, there is no symmetry constraint, therefore a distinction between LB and C modes is not possible (although there might still be a mode mostly polarised orthogonally to the layers, i.e., with a large LB character; this could happen for instance in LMHs).

For a ML-LM with $N > 2$, while the optical activity (discussed in the next section) and the degeneracies do

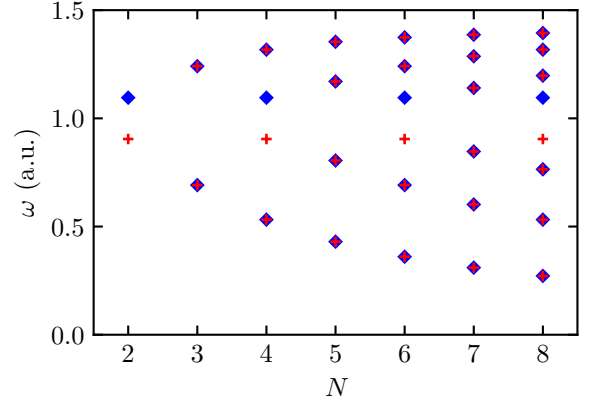


FIG. 3. C-modes fan diagram for ZnCl_2 obtained by solving Eq. (1). The phonon frequency is normalised to the mean of the two frequencies for $N = 2$. Red plus signs and blue diamonds denote C modes along the x and y in-plane directions, respectively. Both B- ZnCl_2 and ML- ZnCl_2 with odd N have tetragonal symmetry, and the two C modes are always degenerate. However, ML- ZnCl_2 with even N have a reduced orthorhombic symmetry, which removes the degeneracy between some of the C modes

TABLE II. Components of the $K_{\alpha\beta}^{(\ell)}$ force-constants tensor (from general symmetry considerations, see Ref. 68) depending on the crystal system of the corresponding 2L-LM formed by layers ℓ and $(\ell + 1)$. The stacking direction is z . Non-zero components are indicated, and components that are equal are indicated with the same name. For monoclinic systems, we need to distinguish the case where the unique axis is in plane (here arbitrarily chosen as y) or along z

tetragonal, hexagonal or trigonal	$\begin{pmatrix} xx & 0 & 0 \\ 0 & xx & 0 \\ 0 & 0 & zz \end{pmatrix}$
orthorhombic	$\begin{pmatrix} xx & 0 & 0 \\ 0 & yy & 0 \\ 0 & 0 & zz \end{pmatrix}$
monoclinic (y): in-plane unique axis	$\begin{pmatrix} xx & 0 & xz \\ 0 & yy & 0 \\ xz & 0 & zz \end{pmatrix}$
monoclinic (z): out-of-plane unique axis	$\begin{pmatrix} xx & xy & 0 \\ xy & yy & 0 \\ 0 & 0 & zz \end{pmatrix}$
triclinic	$\begin{pmatrix} xx & xy & xz \\ xy & yy & yz \\ xz & yz & zx \end{pmatrix}$

depend only on the point group of the ML-LM (as obtained in Sec. II B), in general the considerations of the previous paragraph on when we can define pure C and LB modes cannot be naively applied (see Appendix E for more details and an example).

Since not only G_N often differs from G_b (e.g., in MoS_2 , hBN), but it might also belong to another crystal system, the degeneracies of the modes might be different in B-LM and ML-LM. For instance (see also Appendix D), B-

WTe₂ is orthorhombic (space group Pmn2₁, Hall number 155), but for all N the ML-WTe₂ point group is always m , a monoclinic point group. In other cases, this occurs only for some values of N , like for ZnCl₂ (tetragonal bulk, Hall number 420), where the ML-LM point group is $\bar{4}2m$ (tetragonal) for odd N , but is mmm (orthorhombic) for even N . The degeneracies vary with N in this case, as illustrated in Fig. 3, and can be used as an additional fingerprint of the material.

D. Optical activity of a multilayer

Once the point group of a ML-LM and its normal modes (frequencies and eigenvectors) are known (thanks to the results of the previous sections), one can assess its Raman or IR activity. This can be done by projecting the normal modes onto the different irreducible representations of the point group (listed in standard crystallography references[69–71]) to understand which one they belong to. In particular, apart from accidental degeneracies, a normal mode belongs to one and only one irreducible representation[72], provided that pairs of complex representations that are conjugate of each other are grouped together because of time-reversal symmetry. Thus, the following expectation value will be one for the irreducible representation γ , with characters $\chi^{(\gamma)}(g)$, to which the normal mode (ν, n) belongs, and will be zero for all other representations[72]:

$$p_\gamma(\nu, n) = \frac{d_\gamma}{h} \sum_{g \in G} [\chi^{(\gamma)}(g)]^* \mathbf{U}^{(\nu, n)\dagger} \hat{O}_g \mathbf{U}^{(\nu, n)}, \quad (4)$$

where $\mathbf{U}^{(\nu, n)}$ is a vector collecting the displacements $\mathbf{u}^{(\nu, n)}(\ell)$ of the layers obtained by solving Eq. (2), d_γ is the dimension of the representation, h the order of the point group, and \hat{O}_g the operator associated with the symmetry element g (all these are tabulated for all point groups). From the knowledge of the representation γ for which $p_\gamma(\nu, n) = 1$, we can determine if the mode is Raman and/or IR active depending on whether the representation transforms as the components of a vector (x, y, z) or of a quadratic form (x^2, y^2, xz, \dots) , respectively. Additionally, if there exists at least one quadratic form associated with γ that does not involve the z coordinate, the mode should also be visible in a back-scattering Raman geometry, as the light polarisation vector in a back-scattering experiment with light propagating along z cannot have a z component.

To showcase the application of the method, Tables IV,V report the results obtained for all point groups, when a single force-constant tensor is sufficient, so that the analytical expressions of Sec. II C can be adopted. In particular, for each mode of a N -layer ML-LM with point group G_N , we indicate the irreducible representation to which it belongs together with its IR/Raman activity, and whether the mode visible in a Raman spectroscopy experiment with a back-scattering geometry. The full

analysis for any input LM, also when more than one force-constant tensor is needed, is performed by our online tool (see Sec. IV).

III. RESULTS

We now show with a few examples how to use this approach to reconstruct the fan diagram and the pattern of modes detectable in IR or Raman spectroscopy.

Let us start from the case of MoS₂ and black phosphorous (BP). As discussed in Sec. II B, the ML point group is $\bar{6}m2$ for odd N and $\bar{3}m$ for even N .

Figs. 4a,b plot the fan diagrams for the C and LB modes of ML-MoS₂ as a function of N , where the assignment of the modes is obtained by considering the appropriate entries in Tables IV,V, and reproduce the experiments in Refs. 30 and 34.

We then consider ML-BP whose bulk space group is $A2_1/b2/m2/a$ (space group 64, Hall number 306 when considering the shortest in-plane vector along the second axis), $n_c = 2$ and the corresponding ML-BP point group is mmm both for even and odd N . Figs. 4c,4d report the corresponding fan diagrams, reproducing the experiments of Ref. 46. We note that, in this case, C modes are not visible in back-scattering, consistent with Ref. 46.

As a further example, Fig. 5 shows the fan diagram of PtO₂, which can crystallise in at least two different allotropes differing only in the layer-stacking sequence[73]. One phase has space group $P6_3mc$ (space group 186, Hall number 480) with $n_c = 2$; the other has $n_c = 1$ and space group $P\bar{3}m1$ (space group 164, Hall number 456). In the first case, the ML-PtO₂ point group is always $3m$ as reported in Table III, so that all C and LB modes are Raman-active in back-scattering (see Tables IV,V). In the second case, the point group is $\bar{3}m$ for every N , and the pattern of Raman-active modes is in Figs. 5c,d. Since the pattern is different from the first phase, this implies that the pattern of Raman-active modes detectable in back-scattering can be used as a fingerprint to recognise the stacking sequence and symmetry properties of a given ML-PtO₂.

IV. ONLINE TOOL

In order to make the algorithm described in this paper readily available to any researcher, we implemented it in an online web tool, published on the Materials Cloud web platform[52] at the address <https://materialscloud.org/work/tools/layer-raman-ir>. This tool does not require any installation and works directly in the browser. In the first selection page, shown in Fig. 6a, the user can upload the bulk crystal structure of a LM in a number of common formats, leveraging the parsers implemented in the ASE[74] and pymatgen[75] libraries. A “skin factor” parameter f can also be selected to tune the bond-detection algorithm. In particular, the tool considers two

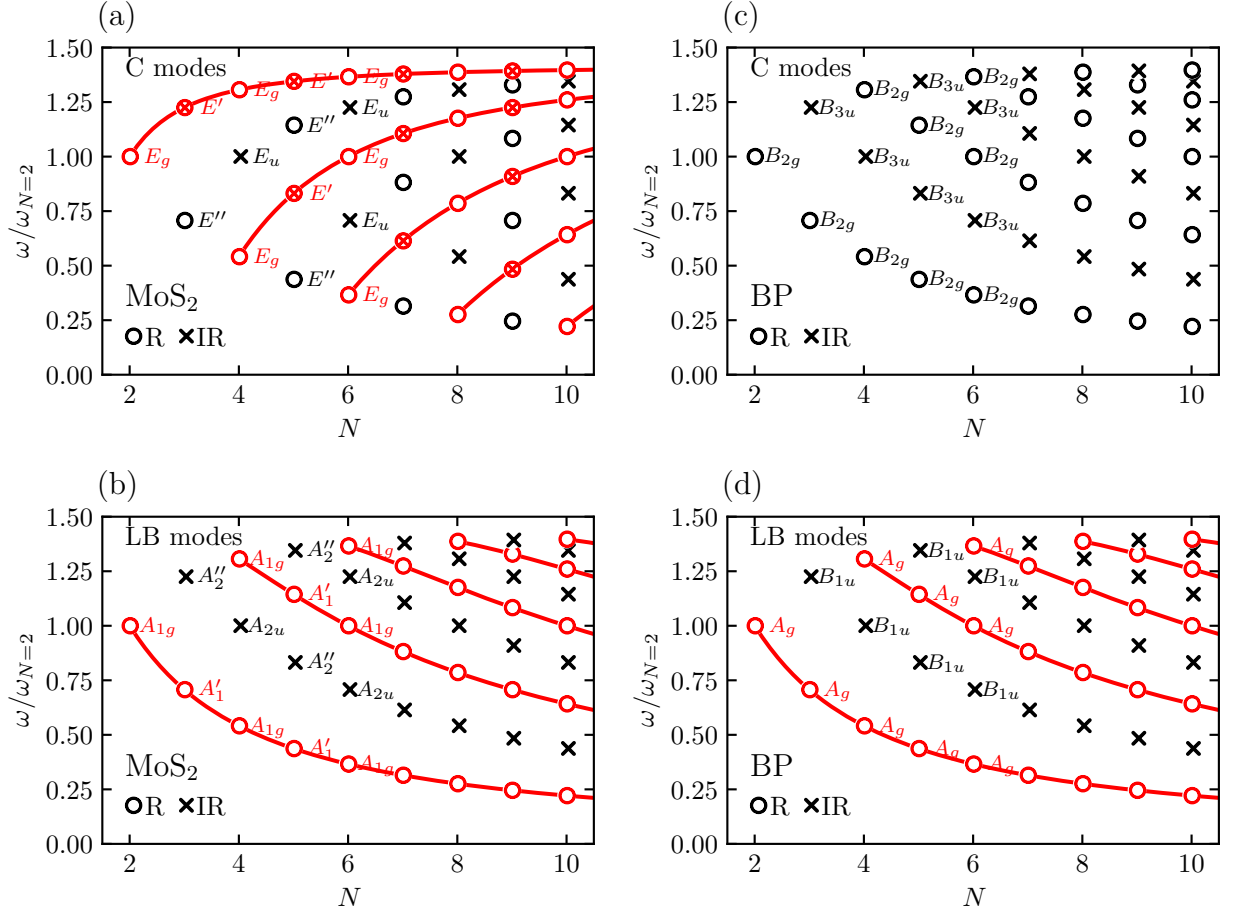


FIG. 4. Fan diagram for C modes (panels a, c) and LB modes (panels b, d) for ML-MoS₂ (panels a, b) and ML-BP (panels c, d). Open circles indicate Raman-active modes, while crosses indicate IR-active modes. Red symbols denote Raman-active modes that are detectable in a back-scattering geometry. For each mode with $N \leq 6$, the corresponding irreducible representation of the point group is reported (note that in the case of ML-BP two non-degenerate sets of C modes exist but only one of them is reported with the corresponding irreducible-representation names). Red lines are guides to the eye, following the pattern of Raman-active modes visible in back-scattering. The frequency ω on the y axis is normalised to the frequency $\omega_{N=2}$ of the corresponding mode in 2L. This frequency is different between C and LB modes

atoms A and B bonded if their distance is $< f \cdot (r_A + r_B)$, where r_A and r_B are the corresponding covalent atomic radii from Ref. 76. Alternatively, it is possible to choose among a few selected examples that we provide as demonstrators.

Once the bulk structure is selected or uploaded, the tool performs computations in the background and produces an output page. It first computes the bonds and then detects the disconnected lower-dimensional components. Once these are determined, it checks that all these components are two-dimensional and identical between them (using the pymatgen code[75] and, in particular, the `structure_matcher` module, to compare layers, check if they are identical within a numerical threshold, and determine which coincidence operation brings one onto the other). It then rotates the whole structure so that the stacking axis is along z and computes the coincidence operation between each pair of layers in the conventional

cell, verifying that the system satisfies the hypotheses of this paper (same coincidence operation between any pair of consecutive layers) and assigning it to one of the three categories of Fig. 1. If any of the previous steps does not succeed, the tool displays a message informing that the structure does not satisfy the assumptions of this work. After this geometry analysis, the tool determines the symmetry of B-LM and 2L-LM, thus the number and shape of the force-constant matrices. Extending the assumptions used here to produce Tables IV,V, the tool works also in the case in which the force constant K and the rotational part of the coincidence operation R do not commute, such as for instance in WTe₂ and ZnCl₂, where force-constant matrices between successive layer pairs are related by symmetry but are not identical. The output page then includes relevant information on the structure (interactive visualisations of B-LM and of 1L-LM, information on the coincidence operation), and

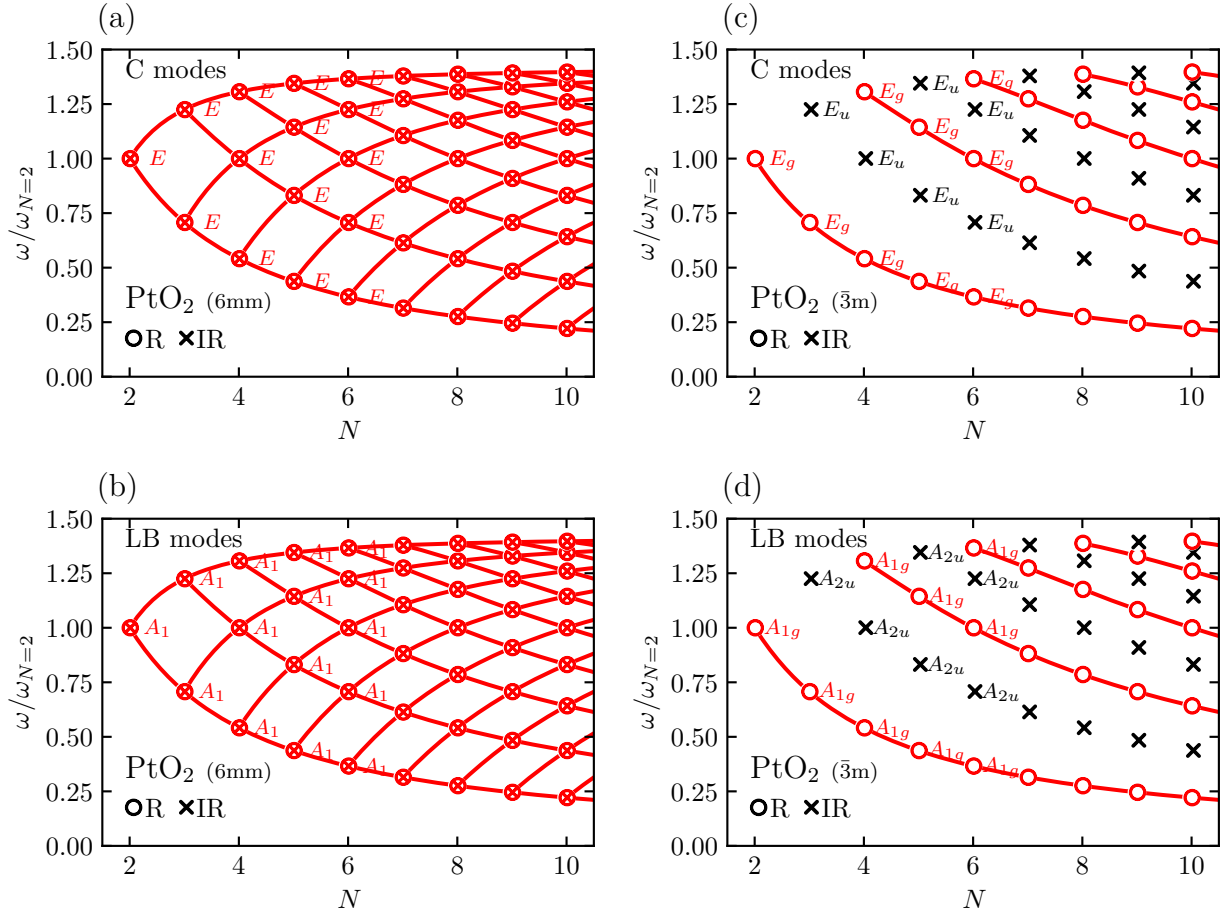


FIG. 5. Fan diagram for C modes (panels a, c) and LM modes (panels b, d) of ML PtO₂ for two different bulk allotropes with space group P6₃mc (panels a, b, point group 6mm) and P3̄m1 (panels c, d, point group 3̄m). See Fig. 4 for the meaning of the symbols and the colours

shows the independent components of the force-constant matrices. An initial random value for these components is provided, chosen to be in the range of those typically occurring in LMs, but these can be changed interactively (e.g., to fit experimental data, or to use values obtained from first principles). The tool then computes the corresponding fan diagram, including the optical activity for IR and Raman spectroscopy. Multiple units are supported both for the force constants and for the phonon frequencies. A screenshot of the resulting fan diagram as provided by the tool (including the section to select the force-constant parameters) is in Fig. 6b.

V. CONCLUSIONS

We presented an approach to seamlessly predict the spectroscopic fingerprints of layered materials composed of repetitions of the same layer. We explained how to obtain, using symmetry arguments, the point group of a finite multilayer, knowing the space group and the Hall setting of the bulk, and provided a table for all possible

space groups and settings. We derived the vibrational modes for any number of layers using a tensorial linear chain model. We then exploited these results to associate each normal mode to a given irreducible representation of the point group of the multilayer, in order to assess the corresponding optical activity, and thus obtain the fan diagram and the pattern of modes that are detectable in IR and Raman spectroscopy. We demonstrated with various examples that this can distinguish different stacking sequences of a given layered material and provides stringent conditions on the symmetry properties of multilayers.

We also provided an easy-to-use online web tool that allows users to upload a bulk multilayer system of their choice (accepting a variety of common crystal-structure formats) and performs all needed operations described in this paper to obtain and display interactively the corresponding fan diagram, even beyond some of the approximations used in this paper (like those used in Tables IV,V). The tool is available on the Materials Cloud web platform[52] at the address <https://materialscloud.org/work/tools/layer-raman-ir> and it is fully open-source

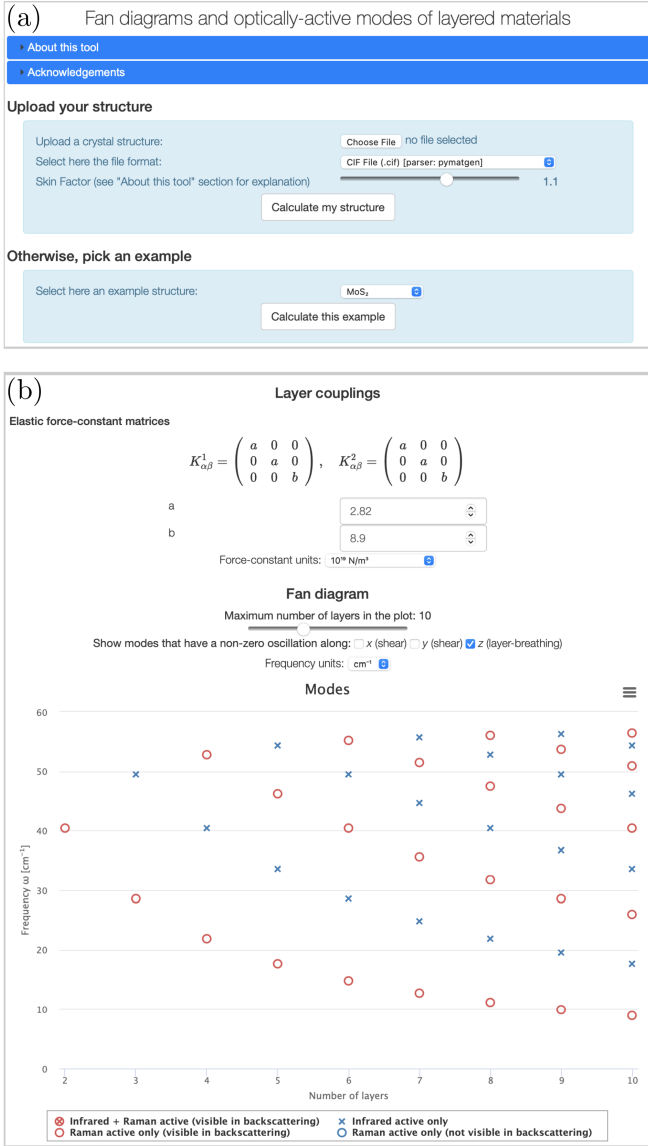


FIG. 6. Screenshots of the online tool implementing the algorithms of this paper, available on the Materials Cloud [52] Work/Tools section. (a) Selection page, where it is possible to upload a structure in a number of common formats, or to select an example. (b) Part of the output page showing the resulting fan diagram for a material, in this case for MoS₂, where the option to display only LB modes has been selected. The output page of the tool actually displays much more information, like visualisations of the crystal structure of B-LM and of the layers, the coincidence operation of the ML-LM, and the symmetry analysis for the B-LM, 1-LM, and ML-LM for all possible values of N

(the code can be found at <https://github.com/epfl-theos/tool-layer-raman-ir>). This will guide computational and experimental researchers interested in studying or interpreting fan diagrams of layered materials.

ACKNOWLEDGEMENTS

We greatly acknowledge Radovan Černý for useful discussions and Leopold Talirz for help in deploying the tool on the Materials Cloud. We acknowledge funding from the MARVEL National Centre of Competence in Research (SNSF) (grant agreement ID 51NF40-182892), from the European Centre of Excellence MaX “Materials design at the Exascale” (grant no. 824143), from the swissuniversities P-5 “Materials Cloud” project (grant agreement ID 182-008), from the EPFL Open Science Fund via the OSSCAR project, from the Graphene Flagship, ERC Grant Hetero2D, and EPSRC Grants EP/509K01711X/1, EP/K017144/1, EP/N010345/1, EP/M507799/5101 and EP/L016087/1, from the Italian Ministry for University and Research through the Levi-Montalcini program, and from SNSF through the Ambizione program (grant 174056).

Appendix A: Compatibility relations of fractional translations

A fractional translation τ is a non-zero translation part of a space group transformation, that is by convention applied after the rotation matrix R , so that the coordinate transformation then reads:

$$\mathbf{r} \rightarrow R\mathbf{r} + \tau. \quad (\text{A1})$$

Since we focus on LMs stacked along the z axis, we consider only the τ_z component of the fractional translation vector. In order for an operation with a non-zero fractional translation to be compatible with a LM with n_c layers in the conventional cell, the product $n_c \cdot \tau_z$ must be an integer: e.g., if we consider a space group with a 3₁ screw axis along z , it might be possible to construct a LM with this space group having 3, 6, ... layers in the B-LM conventional cell, but it is not possible to define a ML system having $n_c = 1, 2, 4, 5, \dots$. In Table III we indicate therefore with a slash (/) any space group that contains at least one incompatible operation for a given value of n_c .

Non-vanishing fractional translations (in the case of MDO polytypes) are therefore admissible only when $n_c = 2, 3, 4, 6$. This follows from the usual crystallographic conditions for which, for e.g., if we rotate a layer by an arbitrary angle, the next layer cannot be periodic with the same unit cell except for a few angles (see Chapters 1 and 2 of Ref. 63).

Appendix B: Grouping fractional translations of LOC operations: Category I

As discussed in the main text, in order to obtain G_N for a ML-LM we need to identify the B-LM LOC operations

compatible with a ML with a given N . These, together with the elements of the layer-invariant point group G_I , will form the G_N group that we seek for.

We now consider independently the 3 categories of Fig. 1. In Category II, there are no LOC operations, therefore $G_N = G_I$. We focus in the rest of this Appendix on Category I and we show in the next Appendix that for Category III we can adapt the results of Category I.

We consider the subset of LOC operation of a given space group (and setting), defined as those that swap the orientation of the z axis, i.e., where the third column of the rotation matrix R is the vector $(0, 0, -1)$. Focusing only on the third coordinate z of a coordinate vector \mathbf{r} and using Eq. (A1), the transformation will therefore read:

$$z \rightarrow -z + \tau_z. \quad (\text{B1})$$

Let us first fix the origin of our coordinate system by setting the origin on the inversion plane of the i -th LOC operation, which will then have no fractional translation along the vertical direction ($\tau_z^i = 0$).

If we now choose another LOC operation, say the j -th, we might need to associate with it a non-zero fractional translation τ_z^j along the vertical direction. In order to connect the coordinate of the inversion planes \tilde{z}_j for this j -th LOC to its fractional translation τ_z^j , we note that the j -th transformation can be equivalently interpreted as the combination of the following operations: 1) translating one inversion plane at $z = \tilde{z}_j$ to $z = 0$ with a transformation $z \rightarrow z - \tilde{z}_j$; 2) applying the inversion transformation about the plane that is now at $z = 0$, therefore changing the sign of the z coordinate, so that the combined transformation reads $z \rightarrow -(z - \tilde{z}_j)$; 3) shifting back the inversion plane to its original position by adding \tilde{z}_j to the third coordinate. The total transformation is thus $z \rightarrow -(z - \tilde{z}_j) + \tilde{z}_j = -z + 2\tilde{z}_j$. Comparing this with Eq. (B1), we obtain that the fractional translation τ_z^j must be $\tau_z^j = 2\tilde{z}_j$.

As we discussed earlier (see Fig. 1), for Category I inversion centres can only be on a layer plane or on a middle plane. Having also chosen earlier the origin on one of these planes, the \tilde{z}_j coordinate of any centre (in fractional coordinates) can thus only be at position at position $\tilde{z}_j = k/2n_c$, with $k \in \mathbb{N}$. E.g., in the case of two layers A and B in the conventional cell ($n_c = 2$), centres will be at position $\tilde{z}_j = 0$ (on layer A), $\tilde{z}_j = 1/4$ (between layer A and layer B), $\tilde{z}_j = 1/2$ (on layer B) or $\tilde{z}_j = 3/4$ (between layer B and layer A in the next unit cell). Thus, fractional translations for any inversion plane can only assume values $\tau_z = k/n_c$, with $k \in \mathbb{N}$.

We can then use the information on the fractional translations to group all LOC operations in sets that share the same inversion plane(s), distinguishing in general those operations having $\tau_z = 2h/n_c$ (with $h \in \mathbb{N}$) and thus inversion on a layer plane, from those having $\tau_z = (2h+1)/n_c$, with inversion on a middle plane. If n_c is odd, the two sets are equivalent, i.e., each LOC transformation

with inversion on a layer plane can be also written as an operation with inversion on a middle plane and a different fractional translation. E.g., in the case $n_c = 3$, one of the two groups would be $\{\tau_z = 0, 2/3, 4/3, 6/3 = 2, \dots\}$ and the second $\{\tau_z = 1/3, 3/3 = 1, 5/3, 7/3, \dots\}$. Remembering that adding an integer to τ_z does not change the operation, we have that $4/3$ is equivalent to $1/3$, 2 to 0 , $5/3$ to $2/3$ and so on, so that both sets coincide with $\{0, 1/3, 2/3\}$. If n_c is even, instead, there are two separate sets of fractional translations, giving rise to transformations having inversion either on layer planes or middle planes. E.g., for $n_c = 4$, one such set contains $\{\tau_z = 0, 1/2\}$ and the other $\{\tau_z = 1/4, 3/4\}$.

For each τ_z in one of these sets, we can construct a potential point group $G_N^{\tau_z}$ by adding to G_I all LOC operations with fractional translation τ_z . In order to be consistent with our initial assumption of a layered structure with n_c identical layers per cell and with the same relation between nearest layers (MDO polytypes), all the various possible point groups $G_N^{\tau_z}$ should be identical for all fractional translations belonging to the same set. This stems from the fact that for Category I MDO polytypes all layer planes are equivalent, as well as all middle planes. If this is not the case, we indicate it with a cross (\times) in Table III. E.g., in the case of space group $P\bar{1}$ (Hall number 2) the bulk point group is $\bar{1}$ while the layer-invariant point group G_I is 1. In the case $n_c = 3$, considering LOC operations with fractional translation $\tau_z = 0$ would add the $\bar{1}$ operation and would give rise to point group $G_N^0 = \bar{1}$. However, considering operations with $\tau_z = 1/3$ (or $\tau_z = 2/3$) would give rise to a different point group $G_N^{1/3} = 1$ ($G_N^{2/3} = 1$), since $P\bar{1}$ has no LOC operations with these fractional translations, and thus $G_N^{\tau_z} = G_I$ in this case. These point groups (1 and $\bar{1}$) are not the same and therefore we mark this case with a \times , indicating that it is not possible to construct a ML with symmetry $P\bar{1}$ and $n_c = 3$ identical layers with the same relation between each pair of them.

We summarise the results as follows: if n_c is odd, we can either obtain a \sloperightarrow or a \times , or there will be only one possible value for G_N , independent of the value of N . When n_c is even, the only difference is that in general there can be two possible choices for the point group G_N . Which value is taken in the finite ML depends on the parity of N : the only LOCs compatible with a finite ML are those with symmetry plane at its centre (a middle plane for even N or a layer plane for odd N). Therefore in these cases the two possible point groups alternate as a function of N .

E.g., in the example of Fig. 2, the Hall number is 242 (Hall symbol $P2/c2/m2_1/m$), $n_c = 2$, and $G_I = m$. Since we have a 2_1 vertical axis, n_c can only be even as discussed in Appendix A and in Table III there is a \sloperightarrow for all odd n_c . If we add LOC operations with a given fractional translation to G_I , we obtain point group $G_I = m$ for fractional translations $1/6, 1/4, 1/3, 2/3, 3/4$ and $5/6$ (since there is no additional LOC operation with these fractional translations). We obtain instead $2/m$ for frac-

tional translation 0, and mm2 for fractional translation $1/2$. Therefore, for $n_c = 2$ we have two independent sets of fractional translations ($\{0\}$ and $\{1/2\}$), and we thus obtain the two valid options for G_N : $2/m$ and $mm2$. However, for $n_c = 4$ (and similarly for larger even values of n_c) we obtain a \times , because one set of fractional translations $\{0, 1/2\}$ (that must be equivalent for $n_c = 4$) would instead contain two different point groups $2/m$ and $mm2$.

From pure symmetry considerations it is not possible to establish which of the two point groups takes place for odd or even N , as discussed in Fig. 2, unless something is known for 1L.

Appendix C: Grouping fractional translations of LOC operations: Category III

If we limit to symmetry considerations (e.g., for the determination of the results of Table III), we note that Category III is equivalent to Category I. Indeed, if we consider a pair of adjacent layers in Category III, these together can be considered as a (now non-polar) “layer” of Category I. In particular, the $\sigma - \rho$ plane between the pairs takes the role of the $\sigma - \rho$ middle plane of Category I, and the $\sigma - \rho$ plane between the layers of the pair takes the role of the $\lambda - \rho$ layer plane of Category I. Note that there are two ways of pairing adjacent layers, and changing such choice swaps the role of middle planes and layer planes.

Intuitively, we can understand why these two categories are equivalent with the following *gedankenexperiment*: if the chemical bonding between the two layers in a pair becomes stronger, without changing the atomic positions (and so without any change to the symmetry of the system), we will eventually end up considering both layers in the pair to be chemically bonded, therefore part of the same rigid layer. In this case, then, we would have considered the system as belonging to category I. Therefore, for the purpose of knowing the possible point groups, Table III can still be used, with the caveat that now n_c indicates the number of pairs of layers for category III.

We emphasise, however, that a separate treatment is needed when we consider the force constants between layers. In this case, the strength of the chemical bonds matters in determining which layers can be considered as moving rigidly, and we need in general to consider two different sets of force constants for the various $\sigma - \rho$ planes of Category III.

In conclusion, for determining the point group of a ML with N layers, there are now the following options:

- N is odd. In this case, on one of the two terminations there is only one layer in a pair. The ML loses all LOC symmetries, and $G_N = G_I$.
- N is even. We can then map this case to Category I, considering a system with $\tilde{N} = N/2$ pairs of layers

as discussed above. Depending on the parity of n_c (which now indicates the number of pairs of layers in the conventional cell) we might have only one or two possibilities for the resulting point group G_N . The termination of the finite ML will uniquely determine how to pair together adjacent layers.

Therefore, for Category III, there might be up to three different point group values as a function of N .

Finally, also “dimerised” systems with non-polar layers, where the interlayer distance alternates (A/B/A/B/...), are still MDO polytypes and behave like those of Category III, and the symmetry plane of the $\sigma - \rho$ coincidence operation does not coincide with the layer plane. We do not consider them explicitly here (and they are quite unlikely to occur in real ML systems) but the online tool is able to correctly consider also these and mark them as Category III.

Appendix D: Point group of ML-LMs with $N < n_p$

In the main text we have focused the discussion on the case $N \geq n_p$. In this case, we can deduce G_N starting from G_b and removing the operations that are not valid in a ML-LM composed of N layers. The operations that remain form G_N , therefore G_N is always a subgroup of G_b .

If $N < n_p$, this group-subgroup relation is, in general, not valid anymore: when looking at the point group, e.g., of a 1L, we have less conditions to satisfy (in particular, we remove the constraints on the specific stacking order of the layers). Therefore, in general, the 1L point group could have more operations than the ML. The example of ML graphite and graphene is discussed in the main text. As another example, we consider WTe_2 , as discussed in the caption of Fig. 7.

Appendix E: An orthorhombic system where modes are not purely LB or C

We now consider the system of Fig. 2a. 2L-LM has point group $2/m$ (monoclinic, as any ML-LM with even N), while MLs with odd N are orthorhombic. By inspecting the crystal structure, we deduce that the unique axis of the 2L-LM is along y . Therefore (see Table II), the force-constant tensor for 2L-LM has the form:

$$K_{\alpha\beta}^{(1)} = \begin{pmatrix} K_{11} & 0 & K_{31} \\ 0 & K_{22} & 0 \\ K_{31} & 0 & K_{33} \end{pmatrix} \quad (E1)$$

for some non-zero values of the parameters K_{11} , K_{22} , K_{33} and K_{31} .

In addition, the coincidence operation can be written, e.g., as a mirror orthogonal to x followed by a translation

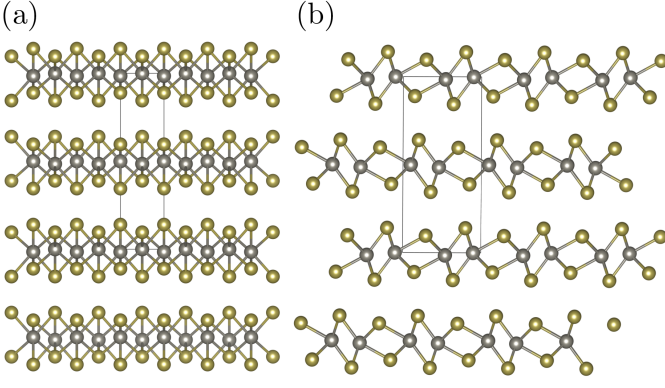


FIG. 7. ML-WTe₂ (COD[60] entry ID 2310355; grey: W, yellow: Te). (a) Side view ($x-z$ projection). (b) Side view ($y-z$ projection). B-WTe₂ has space group Pmn2₁ (number 31) with two layers both in the conventional and the primitive unit cells ($n_c = n_p = 2$; the unit cell is shown); G_b is $mm2$ (C_{2v}). With the given choice of axes the Hall setting is 155 (Pmn2₁), with a mirror plane orthogonal to x , a glide plane orthogonal to y , and a 2₁ screw axis along z . 1L-WTe₂ has space group P2₁/m (with inversion symmetry and a 2₁ screw axis along x), thus $G_{N=1}$ is 2/m (C_{2h}). There is no group-subgroup relation between $mm2$ and 2/m. From Table III, for $N \geq 2$, the point group of any ML-WTe₂ is $G_N = m$ (a subgroup both of $mm2$ and of 2/m). Inversion symmetry (and the horizontal 2₁ screw axis) are lost for any ML-WTe₂ for the given stacking with a B-WTe₂ orthorhombic cell (they might be retrieved with a different stacking having an appropriate a monoclinic cell)

along z , so that its rotational part is:

$$R = \begin{pmatrix} -1 & 0 & 0 \\ 0 & -1 & 0 \\ 0 & 0 & 1 \end{pmatrix}. \quad (\text{E2})$$

This is not the only way to write the coincidence operation: composing it with any bulk operation still provides a valid coincidence operation. The results discussed below, however, are independent of the specific choice.

R and $K^{(1)}$ do not commute, therefore (see Sec. II C) force constants alternate at each interface, taking the values $K^{(1)}$ and $K^{(2)}$, the latter being defined as:

$$K^{(2)} = RK^{(1)}R^{-1} = \begin{pmatrix} K_{11} & 0 & -K_{31} \\ 0 & K_{22} & 0 \\ -K_{31} & 0 & K_{33} \end{pmatrix}. \quad (\text{E3})$$

We first observe that, if we limit to the 1×1 block along y , we can consider R and K as commuting. Therefore, there will be a mode with pure oscillations along y , i.e., a pure C mode.

Let us now focus only on the xz subspace, and define the xz sub-blocks of $K^{(1)}$ and $K^{(2)}$ as:

$$\hat{K}^{(1)} = \begin{pmatrix} K_{11} & K_{31} \\ K_{31} & K_{33} \end{pmatrix}, \quad \hat{K}^{(2)} = \begin{pmatrix} K_{11} & -K_{31} \\ -K_{31} & K_{33} \end{pmatrix}. \quad (\text{E4})$$

We first note that, in 2L-LM, the x and z component mix (due to the off-diagonal K_{31} component), so that, as expected for a monoclinic system, we cannot define pure LB or C modes. The same happens for all even N (monoclinic). One might expect that for odd N , since the point group is instead orthorhombic, x (LB) and z (C) modes would perfectly decouple. However, this is not the case. This can be verified by defining a displacement vector $\mathbf{U} = (u_x(1), u_z(1), u_x(2), u_z(2), \dots, u_x(N), u_z(N))^T$ so that the equation of motion Eq. (1) can be written as $-M\omega_n^2\mathbf{U} = \hat{K}\mathbf{U}$, with \hat{K} having the following block form:

$$\hat{K} = \begin{pmatrix} -\hat{K}^{(1)} & \hat{K}^{(1)} & 0 & \dots & 0 \\ \hat{K}^{(1)} & -\hat{K}^{(0)} & \hat{K}^{(2)} & 0 & \dots & 0 \\ 0 & \hat{K}^{(2)} & -\hat{K}^{(0)} & \hat{K}^{(1)} & 0 & \dots & 0 \\ \vdots & & & \ddots & & & \\ 0 & \dots & & & \hat{K}^{(i)} & -\hat{K}^{(i)} \end{pmatrix} \quad (\text{E5})$$

where $\hat{K}^{(0)} = \hat{K}^{(1)} + \hat{K}^{(2)}$ and $i = 1$ for even N , while $i = 2$ for odd N .

Even if the $\hat{K}^{(0)}$ block is diagonal, there are still mixed xz components in the off-diagonal $\hat{K}^{(1)}$ and $\hat{K}^{(2)}$ blocks, and thus (independently of the parity of N) all eigenvectors have non-zero x and z components. Nevertheless, for odd N (orthorhombic) the matrix \hat{K} commutes with the mirror operation orthogonal to z at the centre of the ML, therefore eigenvectors can be chosen to be simultaneously eigenvectors also of this mirror operation (while this is not the case for even N). Thus, the eigenvectors respect the orthorhombic symmetry of MLs with odd N , and the optical activity is given by the irreducible representations of the corresponding orthorhombic point group.

In summary, even in the orthorhombic case we cannot define purely LB and C modes (on the xz subspace) and, more generally, the decoupling of the modes is determined by the crystal symmetry of 2L-LM, not of the full ML-LM. The optical activity, on the other hand, is determined by the point group of the full ML-LM as discussed in the main text.

Appendix F: Worked-out example: activity for group 2/m

We now consider how to obtain the classification of the optical activity of the modes in the example of Fig. 2a with $N = 4$. The symmetry of this system is described in Appendix E (ML-LM point group 2/m), and the four symmetry operations are: 1 (identity), 2 (180 degrees rotation about the y axis), $\bar{1}$ (inversion) and m (mirror plane, orthogonal to the y axis).

There are two force-constant tensors, $K^{(1)}$ and $K^{(2)}$ in Eqs. (E1), (E3), that alternate. However, if we limit to the 1×1 subspace for the decoupled C mode with oscillations along y , only a single component K_{22} is sufficient to describe the force between any pair of layers. We can

therefore, for this specific case, use the model in Sec. II C, limiting to $\alpha = \beta = 2$ (y axis). The final equation of motion can be written in matrix form as:

$$\omega_n^2 \mathbf{U} = \frac{k}{M} \begin{pmatrix} 1 & -1 & 0 & 0 \\ -1 & 2 & -1 & 0 \\ 0 & -1 & 2 & -1 \\ 0 & 0 & -1 & 1 \end{pmatrix} \mathbf{U} \quad (\text{F1})$$

where, as in the main text, we assume a harmonic form for $u(\ell, t) = u(\ell)e^{i\omega_n t}$, so that $\ddot{u}(\ell, t) = -\omega_n^2 u(\ell, t)$; \mathbf{U} is the column vector of the displacements along y for each layer, i.e., $\mathbf{U} = (u_y(\ell = 1), u_y(\ell = 2), u_y(\ell = 3), u_y(\ell = 4))^T$; and $k = K_{22}$.

Eq. (F1) is a eigenvector equation with eigenvalues ω_n^2 , and can be solved to find the following 4 solutions ($\mathbf{U}^{(n)}$ being the corresponding eigenvectors):

$$\begin{cases} \omega_1^2 = 0, & \mathbf{U}^{(1)} = (\frac{1}{2}, \frac{1}{2}, \frac{1}{2}, \frac{1}{2})^T \\ \omega_2^2 = (2 - \sqrt{2}) \frac{k}{M}, & \mathbf{U}^{(2)} = (v', v'', -v'', -v')^T \\ \omega_3^2 = 2 \frac{k}{M}, & \mathbf{U}^{(3)} = (\frac{1}{2}, -\frac{1}{2}, -\frac{1}{2}, \frac{1}{2})^T \\ \omega_4^2 = (2 + \sqrt{2}) \frac{k}{M}, & \mathbf{U}^{(4)} = (-v'', v', -v', v'')^T \end{cases}, \quad (\text{F2})$$

with $v' = \sqrt{\frac{2+\sqrt{2}}{8}}$ and $v'' = \sqrt{\frac{2-\sqrt{2}}{8}}$. The frequencies are the same as those obtained from Eq. (3).

Now that we have the eigenvectors $\mathbf{U}^{(n)}$, in order to apply Eq. (4) we still need to get the table of the irreducible representations for the point group $2/m$. These are found, e.g., in Refs. 69 and 70:

γ	1	2	$\bar{1}$	m	functions
A_g	1	1	1	1	x^2, y^2, z^2, xy, J_z
B_g	1	-1	1	-1	xz, yz, J_x, J_y
A_u	1	1	-1	-1	z
B_u	1	-1	-1	1	x, y

Appendix G: Tables

TABLE III: Possible ML point groups G_N that can be obtained knowing the space group and Hall number of the corresponding B-LM. Results for all settings compatible with a layered structure (e.g., discarding cubic space groups) and for different n_c in the B-LM conventional cell, for systems of Category I. See Appendices B, C to apply the results of this table to Categories II, III. For each space group all inequivalent settings are considered and labeled by their Hall number. The bulk (G_b) and layer-invariant (G_I) point groups are also provided. / and \times indicate that a LM with given Hall setting and n_c cannot exist with our assumptions of being a MDO polytype (see Appendices A, B for more details). Rhombohedral structures are only considered in their hexagonal setting.

Hall number	Bulk space group	G_b	G_I	Multilayer point group G_N					
				n_c					
				1	2	3	4	5	6
Triclinic									
1	1 (P1)	1	1	1	1	1	1	1	1
2	2 (P $\bar{1}$)	$\bar{1}$	1	$\bar{1}$	1 or $\bar{1}$	\times	\times	\times	\times
Monoclinic									
3	3 (P121)	2	1	2	1 or 2	\times	\times	\times	\times

Continues in the next page...

where the first row indicates the symmetry elements g , and the values in the table are the characters $\chi^{(\gamma)}(g)$ for the 4 irreducible representations $\gamma = A_g, B_g, A_u$ and B_u of $2/m$ (they all have the same dimension $d_\gamma = 1$, and the order of the $2/m$ group is $h = 4$). A_g and B_g are Raman active since they transform as quadratic functions, while A_u and B_u are IR active since they transform as linear functions. Between the two Raman-active representations, only modes corresponding to A_g are visible in a back-scattering geometry, because there are quadratic forms (x^2, y^2, xy) that involve only the x and y coordinates.

Applying Eq. (4) is straightforward, when we note that \hat{O}_1 is the identity; \hat{O}_2 is a 180 degrees rotation with axis along y , so it does not change the sign of displacements along y , but it swaps the order of the layers; $\hat{O}_{\bar{1}}$ changes both the signs of the displacements and the order of the layers; and \hat{O}_m changes the sign of displacements along y but does not change the order of the layers, i.e.:

$$\begin{aligned} \hat{O}_1 \begin{pmatrix} u_1 \\ u_2 \\ u_3 \\ u_4 \end{pmatrix} &= \begin{pmatrix} u_1 \\ u_2 \\ u_3 \\ u_4 \end{pmatrix}, & \hat{O}_2 \begin{pmatrix} u_1 \\ u_2 \\ u_3 \\ u_4 \end{pmatrix} &= \begin{pmatrix} u_4 \\ u_2 \\ u_3 \\ u_1 \end{pmatrix}, \\ \hat{O}_{\bar{1}} \begin{pmatrix} u_1 \\ u_2 \\ u_3 \\ u_4 \end{pmatrix} &= - \begin{pmatrix} u_4 \\ u_3 \\ u_2 \\ u_1 \end{pmatrix}, & \hat{O}_m \begin{pmatrix} u_1 \\ u_2 \\ u_3 \\ u_4 \end{pmatrix} &= - \begin{pmatrix} u_1 \\ u_2 \\ u_3 \\ u_4 \end{pmatrix}. \end{aligned} \quad (\text{F3})$$

Applying Eq. (4), we get that $p_\gamma(n = 2)$ and $p_\gamma(n = 4)$ are 1 only for $\gamma = B_g$ (i.e., Raman active only), while $p_\gamma(n = 3)$ is 1 only for $\gamma = A_u$ (i.e., IR active only). We skip $n = 1$ as this is an acoustic mode with zero frequency where layers translate together of the same amount. These representations correspond to the top row of the $2/m$ (x) case of Table V.

... continues from previous page.

Hall number	Bulk space group	G_b	G_I	Multilayer point group G_N					
				n_c					
				1	2	3	4	5	6
4	3 (P112) <i>Equivalent Hall numbers:</i> 5 (P211) \rightarrow 3	2	2	2	2	2	2	2	2
6	4 (P12 ₁ 1)	2	1	2	1 or 2	\times	\times	\times	\times
7	4 (P112 ₁) <i>Equivalent Hall numbers:</i> 8 (P2 ₁ 11) \rightarrow 6	2	1	/	1	/	1	/	1
9	5 (C121)	2	1	2	1 or 2	\times	\times	\times	\times
11	5 (I121)	2	1	/	2	/	1 or 2	/	\times
12	5 (A112) <i>Equivalent Hall numbers:</i> 10 (A121) \rightarrow 11, 13 (B112) \rightarrow 12, 14 (I112) \rightarrow 12, 15 (B211) \rightarrow 11, 16 (C211) \rightarrow 9, 17 (I211) \rightarrow 11	2	2	/	2	/	2	/	2
18	6 (P1m1)	m	m	m	m	m	m	m	m
19	6 (P11m) <i>Equivalent Hall numbers:</i> 20 (Pm11) \rightarrow 18	m	1	m	1 or m	\times	\times	\times	\times
21	7 (P1c1)	m	1	/	1	/	1	/	1
23	7 (P1a1)	m	m	m	m	m	m	m	m
24	7 (P11a) <i>Equivalent Hall numbers:</i> 22 (P1n1) \rightarrow 21, 25 (P11n) \rightarrow 24, 26 (P11b) \rightarrow 24, 27 (Pb11) \rightarrow 23, 28 (Pn11) \rightarrow 21, 29 (Pc11) \rightarrow 21	m	1	m	1 or m	\times	\times	\times	\times
30	8 (C1m1)	m	m	m	m	m	m	m	m
32	8 (I1m1)	m	m	/	m	/	m	/	m
33	8 (A11m) <i>Equivalent Hall numbers:</i> 31 (A1m1) \rightarrow 32, 34 (B11m) \rightarrow 33, 35 (I11m) \rightarrow 33, 36 (Bm11) \rightarrow 32, 37 (Cm11) \rightarrow 30, 38 (Im11) \rightarrow 32	m	1	/	m	/	1 or m	/	\times
39	9 (C1c1)	m	1	/	1	/	1	/	1
41	9 (I1a1)	m	m	/	m	/	m	/	m
45	9 (A11a) <i>Equivalent Hall numbers:</i> 40 (A1n1) \rightarrow 41, 42 (A1a1) \rightarrow 41, 43 (C1n1) \rightarrow 39, 44 (I1c1) \rightarrow 41, 46 (B11n) \rightarrow 45, 47 (I11b) \rightarrow 45, 48 (B11b) \rightarrow 45, 49 (A11n) \rightarrow 45, 50 (I11a) \rightarrow 45, 51 (Bb11) \rightarrow 41, 52 (Cn11) \rightarrow 39, 53 (Ic11) \rightarrow 41, 54 (Cc11) \rightarrow 39, 55 (Bn11) \rightarrow 41, 56 (Ib11) \rightarrow 41	m	1	/	m	/	1 or m	/	\times
57	10 (P12/m1)	2/m	m	2/m	2/m or m	\times	\times	\times	\times
58	10 (P112/m) <i>Equivalent Hall numbers:</i> 59 (P2/m11) \rightarrow 57	2/m	2	2/m	2 or 2/m	\times	\times	\times	\times
60	11 (P12 ₁ /m1)	2/m	m	2/m	2/m or m	\times	\times	\times	\times
61	11 (P112 ₁ /m) <i>Equivalent Hall numbers:</i> 62 (P2 ₁ /m11) \rightarrow 60	2/m	1	/	$\bar{1}$ or m	/	\times	/	\times
63	12 (C12/m1)	2/m	m	2/m	2/m or m	\times	\times	\times	\times
65	12 (I12/m1)	2/m	m	/	2/m	/	2/m or m	/	\times
66	12 (A112/m) <i>Equivalent Hall numbers:</i> 64 (A12/m1) \rightarrow 65, 67 (B112/m) \rightarrow 66, 68 (I112/m) \rightarrow 66, 69 (B2/m11) \rightarrow 65, 70 (C2/m11) \rightarrow 63, 71 (I2/m11) \rightarrow 65	2/m	2	/	2/m	/	2 or 2/m	/	\times
72	13 (P12/c1)	2/m	1	/	2 or $\bar{1}$	/	\times	/	\times
74	13 (P12/a1)	2/m	m	2/m	2/m or m	\times	\times	\times	\times
75	13 (P112/a) <i>Equivalent Hall numbers:</i> 73 (P12/n1) \rightarrow 72, 76 (P112/n) \rightarrow 75, 77 (P112/b) \rightarrow 75, 78 (P2/b11) \rightarrow 74, 79 (P2/n11) \rightarrow 72, 80 (P2/c11) \rightarrow 72	2/m	2	2/m	2 or 2/m	\times	\times	\times	\times
81	14 (P12 ₁ /c1)	2/m	1	/	2 or $\bar{1}$	/	\times	/	\times
83	14 (P12 ₁ /a1)	2/m	m	2/m	2/m or m	\times	\times	\times	\times
84	14 (P112 ₁ /a) <i>Equivalent Hall numbers:</i> 82 (P12 ₁ /n1) \rightarrow 81, 85 (P112 ₁ /n) \rightarrow 84, 86 (P112 ₁ /b) \rightarrow 84, 87 (P2 ₁ /b11) \rightarrow 83, 88 (P2 ₁ /n11) \rightarrow 81, 89 (P2 ₁ /c11) \rightarrow 81	2/m	1	/	$\bar{1}$ or m	/	\times	/	\times

Continues in the next page...

... continues from previous page.

Hall number	Bulk space group	G_b	G_I	Multilayer point group G_N					
				1	2	3	n_c 4	5	6
90	15 (C12/c1)	2/m	1	/	2 or $\bar{1}$	/	×	/	×
92	15 (I12/a1)	2/m	m	/	2/m	/	2/m or m	/	×
96	15 (A112/a)	2/m	2	/	2/m	/	2 or 2/m	/	×
<i>Equivalent Hall numbers:</i> 91 (A12/n1) → 92, 93 (A12/a1) → 92, 94 (C12/n1) → 90, 95 (I12/c1) → 92, 97 (B112/n) → 96, 98 (I112/b) → 96, 99 (B112/b) → 96, 100 (A112/n) → 96, 101 (I112/a) → 96, 102 (B2/b11) → 92, 103 (C2/n11) → 90, 104 (I2/c11) → 92, 105 (C2/c11) → 90, 106 (B2/n11) → 92, 107 (I2/b11) → 92									
Orthorhombic									
108	16 (P222)	222	2	222	2 or 222	×	×	×	×
109	17 (P222 ₁)	222	1	/	2	/	1 or 2	/	×
110	17 (P2 ₁ 22)	222	2	222	2 or 222	×	×	×	×
<i>Equivalent Hall numbers:</i> 111 (P22 ₁ 2) → 110									
112	18 (P2 ₁ 2 ₁ 2)	222	2	222	2 or 222	×	×	×	×
113	18 (P22 ₁ 2 ₁)	222	1	/	2	/	1 or 2	/	×
<i>Equivalent Hall numbers:</i> 114 (P2 ₁ 22 ₁) → 113									
115	19 (P2 ₁ 2 ₁ 2 ₁)	222	1	/	2	/	1 or 2	/	×
116	20 (C222 ₁)	222	1	/	2	/	1 or 2	/	×
117	20 (A2 ₁ 22)	222	2	/	222	/	2 or 222	/	×
<i>Equivalent Hall numbers:</i> 118 (B22 ₁ 2) → 117									
119	21 (C222)	222	2	222	2 or 222	×	×	×	×
120	21 (A222)	222	2	/	222	/	2 or 222	/	×
<i>Equivalent Hall numbers:</i> 121 (B222) → 120									
122	22 (F222)	222	2	/	222	/	2 or 222	/	×
123	23 (I222)	222	2	/	222	/	2 or 222	/	×
124	24 (I2 ₁ 2 ₁ 2 ₁)	222	2	/	222	/	2 or 222	/	×
125	25 (Pmm2)	mm2	mm2	mm2	mm2	mm2	mm2	mm2	mm2
126	25 (P2mm)	mm2	m	mm2	m or mm2	×	×	×	×
<i>Equivalent Hall numbers:</i> 127 (Pm2m) → 126									
128	26 (Pmc2 ₁)	mm2	m	/	m	/	m	/	m
130	26 (P2 ₁ ma)	mm2	m	mm2	m or mm2	×	×	×	×
<i>Equivalent Hall numbers:</i> 129 (Pcm2 ₁) → 128, 131 (P2 ₁ am) → 130, 132 (Pb2 ₁ m) → 130, 133 (Pm2 ₁ b) → 130									
134	27 (Pcc2)	mm2	2	/	2	/	2	/	2
135	27 (P2aa)	mm2	m	mm2	m or mm2	×	×	×	×
<i>Equivalent Hall numbers:</i> 136 (Pb2b) → 135									
137	28 (Pma2)	mm2	mm2	mm2	mm2	mm2	mm2	mm2	mm2
139	28 (P2mb)	mm2	m	mm2	m or mm2	×	×	×	×
140	28 (P2cm)	mm2	1	/	2 or m	/	×	/	×
<i>Equivalent Hall numbers:</i> 138 (Pbm2) → 137, 141 (Pc2m) → 140, 142 (Pm2a) → 139									
143	29 (Pca2 ₁)	mm2	m	/	m	/	m	/	m
145	29 (P2 ₁ ab)	mm2	m	mm2	m or mm2	×	×	×	×
146	29 (P2 ₁ ca)	mm2	1	/	2 or m	/	×	/	×
<i>Equivalent Hall numbers:</i> 144 (Pbc2 ₁) → 143, 147 (Pc2 ₁ b) → 146, 148 (Pb2 ₁ a) → 145									
149	30 (Pnc2)	mm2	2	/	2	/	2	/	2
151	30 (P2na)	mm2	1	/	2 or m	/	×	/	×
152	30 (P2an)	mm2	m	mm2	m or mm2	×	×	×	×
<i>Equivalent Hall numbers:</i> 150 (Pcn2) → 149, 153 (Pb2n) → 152, 154 (Pn2b) → 151									
155	31 (Pmn2 ₁)	mm2	m	/	m	/	m	/	m
157	31 (P2 ₁ mn)	mm2	m	mm2	m or mm2	×	×	×	×

Continues in the next page...

... continues from previous page.

Hall number	Bulk space group	G_b	G_I	Multilayer point group G_N					
				n_c					
				1	2	3	4	5	6
158	31 (P2 ₁ nm)	mm2	1	/	2 or m	/	×	/	×
<i>Equivalent Hall numbers:</i> 156 (Pnm2 ₁) → 155, 159 (Pn2 ₁ m) → 158, 160 (Pm2 ₁ n) → 157									
161	32 (Pba2)	mm2	mm2	mm2	mm2	mm2	mm2	mm2	mm2
162	32 (P2cb)	mm2	1	/	2 or m	/	×	/	×
<i>Equivalent Hall numbers:</i> 163 (Pc2a) → 162									
164	33 (Pna2 ₁)	mm2	m	/	m	/	m	/	m
166	33 (P2 ₁ nb)	mm2	1	/	2 or m	/	×	/	×
<i>Equivalent Hall numbers:</i> 165 (Pbn2 ₁) → 164, 167 (P2 ₁ cn) → 166, 168 (Pc2 ₁ n) → 166, 169 (Pn2 ₁ a) → 166									
170	34 (Pnn2)	mm2	2	/	2	/	2	/	2
171	34 (P2nn)	mm2	1	/	2 or m	/	×	/	×
<i>Equivalent Hall numbers:</i> 172 (Pn2n) → 171									
173	35 (Cmm2)	mm2	mm2	mm2	mm2	mm2	mm2	mm2	mm2
174	35 (A2mm)	mm2	m	/	mm2	/	m or mm2	/	×
<i>Equivalent Hall numbers:</i> 175 (Bm2m) → 174									
176	36 (Cmc2 ₁)	mm2	m	/	m	/	m	/	m
178	36 (A2 ₁ ma)	mm2	m	/	mm2	/	m or mm2	/	×
<i>Equivalent Hall numbers:</i> 177 (Ccm2 ₁) → 176, 179 (A2 ₁ am) → 178, 180 (Bb2 ₁ m) → 178, 181 (Bm2 ₁ b) → 178									
182	37 (Ccc2)	mm2	2	/	2	/	2	/	2
183	37 (A2aa)	mm2	m	/	mm2	/	m or mm2	/	×
<i>Equivalent Hall numbers:</i> 184 (Bb2b) → 183									
185	38 (Amm2)	mm2	mm2	/	mm2	/	mm2	/	mm2
187	38 (B2mm)	mm2	m	/	mm2	/	m or mm2	/	×
188	38 (C2mm)	mm2	m	mm2	m or mm2	×	×	×	×
<i>Equivalent Hall numbers:</i> 186 (Bmm2) → 185, 189 (Cm2m) → 188, 190 (Am2m) → 187									
191	39 (Abm2)	mm2	mm2	/	mm2	/	mm2	/	mm2
193	39 (B2cm)	mm2	m	/	mm2	/	m or mm2	/	×
194	39 (C2mb)	mm2	m	mm2	m or mm2	×	×	×	×
<i>Equivalent Hall numbers:</i> 192 (Bma2) → 191, 195 (Cm2a) → 194, 196 (Ac2m) → 193									
197	40 (Ama2)	mm2	mm2	/	mm2	/	mm2	/	mm2
199	40 (B2mb)	mm2	m	/	mm2	/	m or mm2	/	×
200	40 (C2cm)	mm2	1	/	2 or m	/	×	/	×
<i>Equivalent Hall numbers:</i> 198 (Bbm2) → 197, 201 (Cc2m) → 200, 202 (Am2a) → 199									
203	41 (Aba2)	mm2	mm2	/	mm2	/	mm2	/	mm2
205	41 (B2cb)	mm2	m	/	mm2	/	m or mm2	/	×
206	41 (C2cb)	mm2	1	/	2 or m	/	×	/	×
<i>Equivalent Hall numbers:</i> 204 (Bba2) → 203, 207 (Cc2a) → 206, 208 (Ac2a) → 205									
209	42 (Fmm2)	mm2	mm2	/	mm2	/	mm2	/	mm2
210	42 (F2mm)	mm2	m	/	mm2	/	m or mm2	/	×
<i>Equivalent Hall numbers:</i> 211 (Fm2m) → 210									
212	43 (Fdd2)	mm2	2	/	/	/	2	/	/
213	43 (F2dd)	mm2	1	/	/	/	2 or m	/	/
<i>Equivalent Hall numbers:</i> 214 (Fd2d) → 213									
215	44 (Imm2)	mm2	mm2	/	mm2	/	mm2	/	mm2
216	44 (I2mm)	mm2	m	/	mm2	/	m or mm2	/	×
<i>Equivalent Hall numbers:</i> 217 (Im2m) → 216									
218	45 (Iba2)	mm2	mm2	/	mm2	/	mm2	/	mm2
219	45 (I2cb)	mm2	m	/	mm2	/	m or mm2	/	×
<i>Equivalent Hall numbers:</i> 220 (Ic2a) → 219									
221	46 (Ima2)	mm2	mm2	/	mm2	/	mm2	/	mm2

Continues in the next page...

... continues from previous page.

Hall number	Bulk space group	G_b	G_I	Multilayer point group G_N					
				1	2	3	n_c 4	5	6
223	46 (I2mb)	mm2	m	/	mm2	/	m or mm2	/	×
	<i>Equivalent Hall numbers:</i> 222 (Ibm2) → 221, 224 (I2cm) → 223, 225 (Ic2m) → 223, 226 (Im2a) → 223								
227	47 (P2/m2/m2/m)	mmm	mm2	mmm	mm2 or mmm	×	×	×	×
228	48 (P2/n2/n2/n)	mmm	2	/	2/m or 222	/	×	/	×
	<i>Equivalent Hall numbers:</i> 229 (P2/n2/n2/n) → 228								
230	49 (P2/c2/c2/m)	mmm	2	/	2/m or 222	/	×	/	×
231	49 (P2/m2/a2/a)	mmm	mm2	mmm	mm2 or mmm	×	×	×	×
	<i>Equivalent Hall numbers:</i> 232 (P2/b2/m2/b) → 231								
233	50 (P2/b2/a2/n)	mmm	mm2	mmm	mm2 or mmm	×	×	×	×
235	50 (P2/n2/c2/b)	mmm	2	/	2/m or 222	/	×	/	×
	<i>Equivalent Hall numbers:</i> 234 (P2/b2/a2/n) → 233, 236 (P2/n2/c2/b) → 235, 237 (P2/c2/n2/a) → 235, 238 (P2/c2/n2/a) → 235								
239	51 (P2 ₁ /m2/m2/a)	mmm	mm2	mmm	mm2 or mmm	×	×	×	×
242	51 (P2/c2/m2 ₁ /m)	mmm	m	/	2/m or mm2	/	×	/	×
	<i>Equivalent Hall numbers:</i> 240 (P2/m2 ₁ /m2/b) → 239, 241 (P2/b2 ₁ /m2/m) → 239, 243 (P2/m2/c2 ₁ /m) → 242, 244 (P2 ₁ /m2/a2/m) → 239								
245	52 (P2/n2 ₁ /n2/a)	mmm	2	/	2/m or 222	/	×	/	×
247	52 (P2/b2/n2 ₁ /n)	mmm	m	/	2/m or mm2	/	×	/	×
	<i>Equivalent Hall numbers:</i> 246 (P2 ₁ /n2/n2/b) → 245, 248 (P2/c2 ₁ /n2/n) → 245, 249 (P2 ₁ /n2/c2/n) → 245, 250 (P2/n2/a2 ₁ /n) → 247								
251	53 (P2/m2/n2 ₁ /a)	mmm	m	/	2/m or mm2	/	×	/	×
253	53 (P2 ₁ /b2/m2/n)	mmm	mm2	mmm	mm2 or mmm	×	×	×	×
254	53 (P2 ₁ /c2/n2/m)	mmm	2	/	2/m or 222	/	×	/	×
	<i>Equivalent Hall numbers:</i> 252 (P2/n2/m2 ₁ /b) → 251, 255 (P2/n2 ₁ /c2/m) → 254, 256 (P2/m2 ₁ /a2/n) → 253								
257	54 (P2 ₁ /c2/c2/a)	mmm	2	/	2/m or 222	/	×	/	×
259	54 (P2/b2 ₁ /a2/a)	mmm	mm2	mmm	mm2 or mmm	×	×	×	×
260	54 (P2/c2/a2 ₁ /a)	mmm	m	/	2/m or mm2	/	×	/	×
	<i>Equivalent Hall numbers:</i> 258 (P2/c2 ₁ /c2/b) → 257, 261 (P2/b2/c2 ₁ /b) → 260, 262 (P2 ₁ /b2/a2/b) → 259								
263	55 (P2 ₁ /b2 ₁ /a2/m)	mmm	mm2	mmm	mm2 or mmm	×	×	×	×
264	55 (P2/m2 ₁ /n2 ₁ /b)	mmm	m	/	2/m or mm2	/	×	/	×
	<i>Equivalent Hall numbers:</i> 265 (P2 ₁ /c2/m2 ₁ /a) → 264								
266	56 (P2 ₁ /c2 ₁ /c2/n)	mmm	2	/	2/m or 222	/	×	/	×
267	56 (P2/n2 ₁ /a2 ₁ /a)	mmm	m	/	2/m or mm2	/	×	/	×
	<i>Equivalent Hall numbers:</i> 268 (P2 ₁ /b2/n2 ₁ /b) → 267								
269	57 (P2/b2 ₁ /c2 ₁ /m)	mmm	m	/	2/m or mm2	/	×	/	×
272	57 (P2 ₁ /m2 ₁ /a2/b)	mmm	mm2	mmm	mm2 or mmm	×	×	×	×
	<i>Equivalent Hall numbers:</i> 270 (P2 ₁ /c2/a2 ₁ /m) → 269, 271 (P2 ₁ /m2/c2 ₁ /a) → 269, 273 (P2 ₁ /b2 ₁ /m2/a) → 272, 274 (P2/c2 ₁ /m2 ₁ /b) → 269								
275	58 (P2 ₁ /n2 ₁ /n2/m)	mmm	2	/	2/m or 222	/	×	/	×
276	58 (P2/m2 ₁ /n2 ₁ /n)	mmm	m	/	2/m or mm2	/	×	/	×
	<i>Equivalent Hall numbers:</i> 277 (P2 ₁ /n2/m2 ₁ /n) → 276								
278	59 (P2 ₁ /m2 ₁ /m2/n)	mmm	mm2	mmm	mm2 or mmm	×	×	×	×
280	59 (P2/n2 ₁ /m2 ₁ /m)	mmm	m	/	2/m or mm2	/	×	/	×
	<i>Equivalent Hall numbers:</i> 279 (P2 ₁ /m2 ₁ /m2/n) → 278, 281 (P2/n2 ₁ /m2 ₁ /m) → 280, 282 (P2 ₁ /m2/n2 ₁ /m) → 280, 283 (P2 ₁ /m2/n2 ₁ /m) → 280								
284	60 (P2 ₁ /b2/c2 ₁ /n)	mmm	m	/	2/m or mm2	/	×	/	×
286	60 (P2 ₁ /n2 ₁ /c2/a)	mmm	2	/	2/m or 222	/	×	/	×
	<i>Equivalent Hall numbers:</i> 285 (P2/c2 ₁ /a2 ₁ /n) → 284, 287 (P2 ₁ /n2/a2 ₁ /b) → 284, 288 (P2/b2 ₁ /n2 ₁ /a) → 284, 289 (P2 ₁ /c2 ₁ /n2/b) → 286								
290	61 (P2 ₁ /b2 ₁ /c2 ₁ /a)	mmm	m	/	2/m or mm2	/	×	/	×

Continues in the next page...

... continues from previous page.

Hall number	Bulk space group	G_b	G_I	Multilayer point group G_N					
				n_c					
1 2 3 4 5 6									
<i>Equivalent Hall numbers:</i> 291 (P ₂₁ /c ₂₁ /a ₂₁ /b) → 290									
292	62 (P ₂₁ /n ₂₁ /m ₂₁ /a)	mmm	m	/	2/m or mm2	/	×	/	×
<i>Equivalent Hall numbers:</i> 293 (P ₂₁ /m ₂₁ /n ₂₁ /b) → 292, 294 (P ₂₁ /b ₂₁ /n ₂₁ /m) → 292, 295 (P ₂₁ /c ₂₁ /m ₂₁ /n) → 292, 296 (P ₂₁ /m ₂₁ /c ₂₁ /n) → 292, 297 (P ₂₁ /n ₂₁ /a ₂₁ /m) → 292									
298	63 (C ₂ /m ₂ /c ₂₁ /m)	mmm	m	/	2/m or mm2	/	×	/	×
300	63 (A ₂₁ /m ₂ /m ₂ /a)	mmm	mm2	/	mmm	/	mm2 or mmm	/	×
<i>Equivalent Hall numbers:</i> 299 (C ₂ /c ₂ /m ₂₁ /m) → 298, 301 (A ₂₁ /m ₂ /a ₂ /m) → 300, 302 (B ₂ /b ₂₁ /m ₂ /m) → 300, 303 (B ₂ /m ₂₁ /m ₂ /b) → 300									
304	64 (C ₂ /m ₂ /c ₂₁ /a)	mmm	m	/	2/m or mm2	/	×	/	×
306	64 (A ₂₁ /b ₂ /m ₂ /a)	mmm	mm2	/	mmm	/	mm2 or mmm	/	×
<i>Equivalent Hall numbers:</i> 305 (C ₂ /c ₂ /m ₂₁ /b) → 304, 307 (A ₂₁ /c ₂ /a ₂ /m) → 306, 308 (B ₂ /b ₂₁ /c ₂ /m) → 306, 309 (B ₂ /m ₂₁ /a ₂ /b) → 306									
310	65 (C ₂ /m ₂ /m ₂ /m)	mmm	mm2	mmm	mm2 or mmm	×	×	×	×
311	65 (A ₂ /m ₂ /m ₂ /m)	mmm	mm2	/	mmm	/	mm2 or mmm	/	×
<i>Equivalent Hall numbers:</i> 312 (B ₂ /m ₂ /m ₂ /m) → 311									
313	66 (C ₂ /c ₂ /c ₂ /m)	mmm	2	/	2/m or 222	/	×	/	×
314	66 (A ₂ /m ₂ /a ₂ /a)	mmm	mm2	/	mmm	/	mm2 or mmm	/	×
<i>Equivalent Hall numbers:</i> 315 (B ₂ /b ₂ /m ₂ /b) → 314									
316	67 (C ₂ /m ₂ /m ₂ /a)	mmm	mm2	mmm	mm2 or mmm	×	×	×	×
318	67 (A ₂ /b ₂ /m ₂ /m)	mmm	mm2	/	mmm	/	mm2 or mmm	/	×
<i>Equivalent Hall numbers:</i> 317 (C ₂ /m ₂ /m ₂ /b) → 316, 319 (A ₂ /c ₂ /m ₂ /m) → 318, 320 (B ₂ /m ₂ /c ₂ /m) → 318, 321 (B ₂ /m ₂ /a ₂ /m) → 318									
322	68 (C ₂ /c ₂ /c ₂ /a)	mmm	2	/	2/m or 222	/	×	/	×
326	68 (A ₂ /b ₂ /a ₂ /a)	mmm	mm2	/	mmm	/	mm2 or mmm	/	×
<i>Equivalent Hall numbers:</i> 323 (C ₂ /c ₂ /c ₂ /a) → 322, 324 (C ₂ /c ₂ /c ₂ /b) → 322, 325 (C ₂ /c ₂ /c ₂ /b) → 322, 327 (A ₂ /b ₂ /a ₂ /a) → 326, 328 (A ₂ /c ₂ /a ₂ /a) → 326, 329 (A ₂ /c ₂ /a ₂ /a) → 326, 330 (B ₂ /b ₂ /c ₂ /b) → 326, 331 (B ₂ /b ₂ /c ₂ /b) → 326, 332 (B ₂ /b ₂ /a ₂ /b) → 326, 333 (B ₂ /b ₂ /a ₂ /b) → 326									
334	69 (F ₂ /m ₂ /m ₂ /m)	mmm	mm2	/	mmm	/	mm2 or mmm	/	×
335	70 (F ₂ /d ₂ /d ₂ /d)	mmm	2	/	/	/	2/m or 222	/	/
<i>Equivalent Hall numbers:</i> 336 (F ₂ /d ₂ /d ₂ /d) → 335									
337	71 (I ₂ /m ₂ /m ₂ /m)	mmm	mm2	/	mmm	/	mm2 or mmm	/	×
338	72 (I ₂ /b ₂ /a ₂ /m)	mmm	mm2	/	mmm	/	mm2 or mmm	/	×
<i>Equivalent Hall numbers:</i> 339 (I ₂ /m ₂ /c ₂ /b) → 338, 340 (I ₂ /c ₂ /m ₂ /a) → 338									
341	73 (I ₂ /b ₂ /c ₂ /a)	mmm	mm2	/	mmm	/	mm2 or mmm	/	×
<i>Equivalent Hall numbers:</i> 342 (I ₂ /c ₂ /a ₂ /b) → 341									
343	74 (I ₂ /m ₂ /m ₂ /a)	mmm	mm2	/	mmm	/	mm2 or mmm	/	×
<i>Equivalent Hall numbers:</i> 344 (I ₂ /m ₂ /m ₂ /b) → 343, 345 (I ₂ /b ₂ /m ₂ /m) → 343, 346 (I ₂ /c ₂ /m ₂ /m) → 343, 347 (I ₂ /m ₂ /c ₂ /m) → 343, 348 (I ₂ /m ₂ /a ₂ /m) → 343									
Tetragonal									
349	75 (P ₄)	4	4	4	4	4	4	4	4
350	76 (P ₄ ₁)	4	1	/	/	/	1	/	/
351	77 (P ₄ ₂)	4	2	/	2	/	2	/	2
352	78 (P ₄ ₃)	4	1	/	/	/	1	/	/
353	79 (I ₄)	4	4	/	4	/	4	/	4
354	80 (I ₄ ₁)	4	2	/	/	/	2	/	/
355	81 (P ₄ [̄])	4̄	2	4̄	2 or 4̄	×	×	×	×

Continues in the next page...

... continues from previous page.

Hall number	Bulk space group	G_b	G_I	Multilayer point group G_N					
				1	2	3	n_c 4	5	6
356	82 ($I\bar{4}$)	$\bar{4}$	2	/	$\bar{4}$	/	2 or $\bar{4}$	/	×
357	83 (P4/m)	4/m	4	4/m	4 or 4/m	×	×	×	×
358	84 (P4 ₂ /m)	4/m	2	/	2/m or $\bar{4}$	/	×	/	×
359	85 (P4/n) <i>Equivalent Hall numbers: 360 (P4/n) → 359</i>	4/m	4	4/m	4 or 4/m	×	×	×	×
361	86 (P4 ₂ /n) <i>Equivalent Hall numbers: 362 (P4₂/n) → 361</i>	4/m	2	/	2/m or $\bar{4}$	/	×	/	×
363	87 (I4/m)	4/m	4	/	4/m	/	4 or 4/m	/	×
364	88 (I4 ₁ /a) <i>Equivalent Hall numbers: 365 (I4₁/a) → 364</i>	4/m	2	/	/	/	2/m or $\bar{4}$	/	/
366	89 (P422)	422	4	422	4 or 422	×	×	×	×
367	90 (P42 ₁ 2)	422	4	422	4 or 422	×	×	×	×
368	91 (P4 ₁ 22)	422	1	/	/	/	2	/	/
369	92 (P4 ₁ 2 ₁ 2)	422	1	/	/	/	2	/	/
370	93 (P4 ₂ 22)	422	2	/	222	/	2 or 222	/	×
371	94 (P4 ₂ 2 ₁ 2)	422	2	/	222	/	2 or 222	/	×
372	95 (P4 ₃ 22)	422	1	/	/	/	2	/	/
373	96 (P4 ₃ 2 ₁ 2)	422	1	/	/	/	2	/	/
374	97 (I422)	422	4	/	422	/	4 or 422	/	×
375	98 (I4 ₁ 22)	422	2	/	/	/	222	/	/
376	99 (P4mm)	4mm	4mm	4mm	4mm	4mm	4mm	4mm	4mm
377	100 (P4bm)	4mm	4mm	4mm	4mm	4mm	4mm	4mm	4mm
378	101 (P4 ₂ cm)	4mm	mm2	/	mm2	/	mm2	/	mm2
379	102 (P4 ₂ nm)	4mm	mm2	/	mm2	/	mm2	/	mm2
380	103 (P4cc)	4mm	4	/	4	/	4	/	4
381	104 (P4nc)	4mm	4	/	4	/	4	/	4
382	105 (P4 ₂ mc)	4mm	mm2	/	mm2	/	mm2	/	mm2
383	106 (P4 ₂ bc)	4mm	mm2	/	mm2	/	mm2	/	mm2
384	107 (I4mm)	4mm	4mm	/	4mm	/	4mm	/	4mm
385	108 (I4cm)	4mm	4mm	/	4mm	/	4mm	/	4mm
386	109 (I4 ₁ md)	4mm	mm2	/	/	/	mm2	/	/
387	110 (I4 ₁ cd)	4mm	mm2	/	/	/	mm2	/	/
388	111 (P $\bar{4}$ 2m)	$\bar{4}$ 2m	mm2	$\bar{4}$ 2m	$\bar{4}$ 2m or mm2	×	×	×	×
389	112 (P $\bar{4}$ 2c)	$\bar{4}$ 2m	2	/	222 or $\bar{4}$	/	×	/	×
390	113 (P $\bar{4}$ 2 ₁ m)	$\bar{4}$ 2m	mm2	$\bar{4}$ 2m	$\bar{4}$ 2m or mm2	×	×	×	×
391	114 (P $\bar{4}$ 2 ₁ c)	$\bar{4}$ 2m	2	/	222 or $\bar{4}$	/	×	/	×
392	115 (P $\bar{4}$ m2)	$\bar{4}$ 2m	mm2	$\bar{4}$ 2m	$\bar{4}$ 2m or mm2	×	×	×	×
393	116 (P $\bar{4}$ c2)	$\bar{4}$ 2m	2	/	222 or $\bar{4}$	/	×	/	×
394	117 (P $\bar{4}$ b2)	$\bar{4}$ 2m	mm2	$\bar{4}$ 2m	$\bar{4}$ 2m or mm2	×	×	×	×
395	118 (P $\bar{4}$ n2)	$\bar{4}$ 2m	2	/	222 or $\bar{4}$	/	×	/	×

Continues in the next page...

... continues from previous page.

Hall number	Bulk space group	G_b	G_I	Multilayer point group G_N						
				1	2	3	n_c 4	5	6	
396	119 ($I\bar{4}m2$)	$\bar{4}2m$	mm2	/	$\bar{4}2m$	/	$\bar{4}2m$ or mm2	/	×	
397	120 ($I\bar{4}c2$)	$\bar{4}2m$	mm2	/	$\bar{4}2m$	/	$\bar{4}2m$ or mm2	/	×	
398	121 ($I\bar{4}2m$)	$\bar{4}2m$	mm2	/	$\bar{4}2m$	/	$\bar{4}2m$ or mm2	/	×	
399	122 ($I\bar{4}2d$)	$\bar{4}2m$	2	/	/	/	222 or $\bar{4}$	/	/	
400	123 ($P4/m2/m2/m$)	4/mmm	4mm	4/mmm	4mm or 4/mmm	×	×	×	×	
401	124 ($P4/m2/c2/c$)	4/mmm	4	/	4/m or 422	/	×	/	×	
402	125 ($P4/n2/b2/m$)	4/mmm	4mm	4/mmm	4mm or 4/mmm	×	×	×	×	
	<i>Equivalent Hall numbers:</i> 403 ($P4/n2/b2/m$) → 402									
404	126 ($P4/n2/n2/c$)	4/mmm	4	/	4/m or 422	/	×	/	×	
	<i>Equivalent Hall numbers:</i> 405 ($P4/n2/n2/c$) → 404									
406	127 ($P4/m2_1/bm$)	4/mmm	4mm	4/mmm	4mm or 4/mmm	×	×	×	×	
407	128 ($P4/m2_1/nc$)	4/mmm	4	/	4/m or 422	/	×	/	×	
408	129 ($P4/n2_1/mm$)	4/mmm	4mm	4/mmm	4mm or 4/mmm	×	×	×	×	
	<i>Equivalent Hall numbers:</i> 409 ($P4/n2_1/mm$) → 408									
410	130 ($P4/n2_1/cc$)	4/mmm	4	/	4/m or 422	/	×	/	×	
	<i>Equivalent Hall numbers:</i> 411 ($P4/n2_1/cc$) → 410									
412	131 ($P4_2/m2/m2/c$)	4/mmm	mm2	/	$\bar{4}2m$ or mmm	/	×	/	×	
413	132 ($P4_2/m2/c2/m$)	4/mmm	mm2	/	$\bar{4}2m$ or mmm	/	×	/	×	
414	133 ($P4_2/n2/b2/c$)	4/mmm	mm2	/	$\bar{4}2m$ or mmm	/	×	/	×	
	<i>Equivalent Hall numbers:</i> 415 ($P4_2/n2/b2/c$) → 414									
416	134 ($P4_2/n2/n2/m$)	4/mmm	mm2	/	$\bar{4}2m$ or mmm	/	×	/	×	
	<i>Equivalent Hall numbers:</i> 417 ($P4_2/n2/n2/m$) → 416									
418	135 ($P4_2/m2_1/b2/c$)	4/mmm	mm2	/	$\bar{4}2m$ or mmm	/	×	/	×	
419	136 ($P4_2/m2_1/n2/m$)	4/mmm	mm2	/	$\bar{4}2m$ or mmm	/	×	/	×	
420	137 ($P4_2/n2_1/m2/c$)	4/mmm	mm2	/	$\bar{4}2m$ or mmm	/	×	/	×	
	<i>Equivalent Hall numbers:</i> 421 ($P4_2/n2_1/m2/c$) → 420									
422	138 ($P4_2/n2_1/c2/m$)	4/mmm	mm2	/	$\bar{4}2m$ or mmm	/	×	/	×	
	<i>Equivalent Hall numbers:</i> 423 ($P4_2/n2_1/c2/m$) → 422									
424	139 ($I4/m2/m2/m$)	4/mmm	4mm	/	4/mmm	/	4mm or 4/mmm	/	×	
425	140 ($I4/m2/c2/m$)	4/mmm	4mm	/	4/mmm	/	4mm or 4/mmm	/	×	
426	141 ($I4_1/a2/m2/d$)	4/mmm	mm2	/	/	/	$\bar{4}2m$ or mmm	/	/	
	<i>Equivalent Hall numbers:</i> 427 ($I4_1/a2/m2/d$) → 426									
428	142 ($I4_1/a2/c2/d$)	4/mmm	mm2	/	/	/	$\bar{4}2m$ or mmm	/	/	
	<i>Equivalent Hall numbers:</i> 429 ($I4_1/a2/c2/d$) → 428									
Trigonal										
430	143 (P3)	3	3	3	3	3	3	3	3	
431	144 (P3 ₁)	3	1	/	/	1	/	/	1	
432	145 (P3 ₂)	3	1	/	/	1	/	/	1	
433	146 (R3)	3	3	/	/	3	/	/	3	
435	147 (P $\bar{3}$)	$\bar{3}$	3	$\bar{3}$	3 or $\bar{3}$	×	×	×	×	
436	148 (R $\bar{3}$)	$\bar{3}$	3	/	/	$\bar{3}$	/	/	3 or $\bar{3}$	
438	149 (P312)	32	3	32	3 or 32	×	×	×	×	

Continues in the next page...

... continues from previous page.

Hall number	Bulk space group	G_b	G_I	Multilayer point group G_N					
				1	2	3	n_c 4	5	6
439	150 (P321)	32	3	32	3 or 32	×	×	×	×
440	151 (P3 ₁ 12)	32	1	/	/	2	/	/	1 or 2
441	152 (P3 ₁ 21)	32	1	/	/	2	/	/	1 or 2
442	153 (P3 ₂ 12)	32	1	/	/	2	/	/	1 or 2
443	154 (P3 ₂ 21)	32	1	/	/	2	/	/	1 or 2
444	155 (R32)	32	3	/	/	32	/	/	3 or 32
446	156 (P3m1)	3m	3m	3m	3m	3m	3m	3m	3m
447	157 (P31m)	3m	3m	3m	3m	3m	3m	3m	3m
448	158 (P3c1)	3m	3	/	3	/	3	/	3
449	159 (P31c)	3m	3	/	3	/	3	/	3
450	160 (R3m)	3m	3m	/	/	3m	/	/	3m
452	161 (R3c)	3m	3	/	/	/	/	/	3
454	162 (P3 ₁ 12/m)	3m	3m	3m	3m or 3m	×	×	×	×
455	163 (P3 ₁ 12/c)	3m	3	/	32 or 3	/	×	/	×
456	164 (P3 ₂ 12/m1)	3m	3m	3m	3m or 3m	×	×	×	×
457	165 (P3 ₂ 12/c1)	3m	3	/	32 or 3	/	×	/	×
458	166 (R3 ₂ 12/m)	3m	3m	/	/	3m	/	/	3m or 3m
460	167 (R3 ₂ 12/c)	3m	3	/	/	/	/	/	32 or 3
Hexagonal									
462	168 (P6)	6	6	6	6	6	6	6	6
463	169 (P6 ₁)	6	1	/	/	/	/	/	1
464	170 (P6 ₅)	6	1	/	/	/	/	/	1
465	171 (P6 ₂)	6	2	/	/	2	/	/	2
466	172 (P6 ₄)	6	2	/	/	2	/	/	2
467	173 (P6 ₃)	6	3	/	3	/	3	/	3
468	174 (P6)	6	3	6	3 or 6	×	×	×	×
469	175 (P6/m)	6/m	6	6/m	6 or 6/m	×	×	×	×
470	176 (P6 ₃ /m)	6/m	3	/	3 or 6	/	×	/	×
471	177 (P622)	622	6	622	6 or 622	×	×	×	×
472	178 (P6 ₁ 22)	622	1	/	/	/	/	/	2
473	179 (P6 ₅ 22)	622	1	/	/	/	/	/	2
474	180 (P6 ₂ 22)	622	2	/	/	222	/	/	2 or 222
475	181 (P6 ₄ 22)	622	2	/	/	222	/	/	2 or 222
476	182 (P6 ₃ 22)	622	3	/	32	/	3 or 32	/	×
477	183 (P6mm)	6mm	6mm	6mm	6mm	6mm	6mm	6mm	6mm
478	184 (P6cc)	6mm	6	/	6	/	6	/	6
479	185 (P6 ₃ cm)	6mm	3m	/	3m	/	3m	/	3m
480	186 (P6 ₃ mc)	6mm	3m	/	3m	/	3m	/	3m
481	187 (P6m2)	6m2	3m	6m2	3m or 6m2	×	×	×	×

Continues in the next page...

... continues from previous page.

Hall number	Bulk space group	G_b	G_I	Multilayer point group G_N					
				1	2	3	n_c 4	5	6
482	188 (P $\bar{6}c2$)	$\bar{6}m2$	3	/	32 or $\bar{6}$	/	×	/	×
483	189 (P $\bar{6}2m$)	$\bar{6}m2$	3m	$\bar{6}m2$	3m or $\bar{6}m2$	×	×	×	×
484	190 (P $\bar{6}2c$)	$\bar{6}m2$	3	/	32 or $\bar{6}$	/	×	/	×
485	191 (P6/m2/m2/m)	6/mmm	6mm	6/mmm	6mm or 6/mmm	×	×	×	×
486	192 (P6/m2/c2/c)	6/mmm	6	/	6/m or 622	/	×	/	×
487	193 (P6 $_3$ /m2/c2/m)	6/mmm	3m	/	$\bar{3}m$ or $\bar{6}m2$	/	×	/	×
488	194 (P6 $_3$ /m2/m2/c)	6/mmm	3m	/	$\bar{3}m$ or $\bar{6}m2$	/	×	/	×

TABLE IV: LBM classification for a N -layer ML to its point group G_N . For a given point group and N , the modes are reported from left to right in order of increasing frequency. Raman active modes are denoted as \circ , IR active ones as \times , while those that are both Raman and IR active as \otimes . A red symbol indicates that the mode can be detected in a backscattering Raman experiment orthogonal to the layers. The irreducible representation to which each mode belongs is also reported. Whenever necessary, different orientations of the principal symmetry element with respect to z are considered and specified in parenthesis. In cases where it is not possible to decouple C and LB modes, we report them noting that the mode assignment coincides with that of the corresponding mixed mode in Table V.

Pointgroup	$N = 2$	$N = 3$	$N = 4$	$N = 5$	$N = 6$	$N = 7$
1	\otimes A	\otimes A	\otimes A	\otimes A	\otimes A	\otimes A
$\bar{1}$	\circ A_g	\circ A_g	\times A_u	\circ A_g	\times A_u	\circ A_g
2 (x)	\otimes A	\otimes A	\otimes B	\otimes A	\otimes B	\otimes A
2 (z)	\otimes A	\otimes A	\otimes A	\otimes A	\otimes A	\otimes A
m (x)	\otimes A'	\otimes A'	\otimes A'	\otimes A'	\otimes A'	\otimes A'
m (z)	\otimes A'	\otimes A'	\otimes A''	\otimes A'	\otimes A''	\otimes A'
2/m (x)	\circ A_g	\circ A_g	\times B_u	\circ A_g	\times B_u	\circ A_g
2/m (z)	\circ A_g	\circ A_g	\times A_u	\circ A_g	\times A_u	\circ A_g
222	\circ A	\circ A	\otimes B_1	\circ A	\otimes B_1	\circ A
mm2 (x)	\otimes A_1	\otimes A_1	\otimes B_2	\otimes A_1	\otimes B_2	\otimes A_1
mm2 (z)	\otimes A_1	\otimes A_1	\otimes A_1	\otimes A_1	\otimes A_1	\otimes A_1
mmm	\circ A_g	\circ A_g	\times B_{1u}	\circ A_g	\times B_{1u}	\circ A_g
4	\otimes A	\otimes A	\otimes A	\otimes A	\otimes A	\otimes A
$\bar{4}$	\circ A	\circ A	\otimes B	\circ A	\otimes B	\circ A
4/m	\circ	\circ	\times	\circ	\times	\circ

Continues in the next page...

... continues from previous page.

Pointgroup	$N = 2$	$N = 3$	$N = 4$	$N = 5$	$N = 6$	$N = 7$
	A_g	A_g A_u	A_g A_u A_g	A_g A_u A_g A_u	A_g A_u A_g A_u A_g	A_g A_u A_g A_u A_g A_u
422	\circ A_1	\circ \times A_1 A_2	\circ \times \circ A_1 A_2 A_1	\circ \times \circ \times A_1 A_2 A_1 A_2	\circ \times \circ \times \circ A_1 A_2 A_1 A_2 A_1	\circ \times \circ \times \circ \times A_1 A_2 A_1 A_2 A_1 A_2
4mm	\otimes A_1	\otimes \otimes A_1 A_1	\otimes \otimes \otimes A_1 A_1 A_1	\otimes \otimes \otimes \otimes A_1 A_1 A_1 A_1	\otimes \otimes \otimes \otimes \otimes A_1 A_1 A_1 A_1 A_1	\otimes \otimes \otimes \otimes \otimes \otimes A_1 A_1 A_1 A_1 A_1 A_1
$\bar{4}2m$	\circ A_1	\circ \otimes A_1 B_2	\circ \otimes \circ A_1 B_2 A_1	\circ \otimes \circ \otimes A_1 B_2 A_1 B_2	\circ \otimes \circ \otimes \circ A_1 B_2 A_1 B_2 A_1	\circ \otimes \circ \otimes \circ \otimes A_1 B_2 A_1 B_2 A_1 B_2
4/mmm	\circ A_{1g}	\circ \times A_{1g} A_{2u}	\circ \times \circ A_{1g} A_{2u} A_{1g}	\circ \times \circ \times A_{1g} A_{2u} A_{1g} A_{2u}	\circ \times \circ \times \circ A_{1g} A_{2u} A_{1g} A_{2u} A_{1g}	\circ \times \circ \times \circ \times A_{1g} A_{2u} A_{1g} A_{2u} A_{1g} A_{2u}
3	\otimes A	\otimes \otimes A A	\otimes \otimes \otimes A A A	\otimes \otimes \otimes \otimes A A A A	\otimes \otimes \otimes \otimes \otimes A A A A A	\otimes \otimes \otimes \otimes \otimes \otimes A A A A A A
$\bar{3}$	\circ A_g	\circ \times A_g A_u	\circ \times \circ A_g A_u A_g	\circ \times \circ \times A_g A_u A_g A_u	\circ \times \circ \times \circ A_g A_u A_g A_u A_g	\circ \times \circ \times \circ \times A_g A_u A_g A_u A_g A_u
32	\circ A_1	\circ \times A_1 A_2	\circ \times \circ A_1 A_2 A_1	\circ \times \circ \times A_1 A_2 A_1 A_2	\circ \times \circ \times \circ A_1 A_2 A_1 A_2 A_1	\circ \times \circ \times \circ \times A_1 A_2 A_1 A_2 A_1 A_2
3m	\otimes A_1	\otimes \otimes A_1 A_1	\otimes \otimes \otimes A_1 A_1 A_1	\otimes \otimes \otimes \otimes A_1 A_1 A_1 A_1	\otimes \otimes \otimes \otimes \otimes A_1 A_1 A_1 A_1 A_1	\otimes \otimes \otimes \otimes \otimes \otimes A_1 A_1 A_1 A_1 A_1 A_1
$\bar{3}m$	\circ A_{1g}	\circ \times A_{1g} A_{2u}	\circ \times \circ A_{1g} A_{2u} A_{1g}	\circ \times \circ \times A_{1g} A_{2u} A_{1g} A_{2u}	\circ \times \circ \times \circ A_{1g} A_{2u} A_{1g} A_{2u} A_{1g}	\circ \times \circ \times \circ \times A_{1g} A_{2u} A_{1g} A_{2u} A_{1g} A_{2u}
6	\otimes A	\otimes \otimes \otimes A A A	\otimes \otimes \otimes A A A	\otimes \otimes \otimes \otimes A A A A	\otimes \otimes \otimes \otimes \otimes A A A A A	\otimes \otimes \otimes \otimes \otimes \otimes A A A A A A
$\bar{6}$	\circ A'	\circ \times A' A''	\circ \times \circ A' A'' A'	\circ \times \circ \times A' A'' A' A''	\circ \times \circ \times \circ A' A'' A' A'' A'	\circ \times \circ \times \circ \times A' A'' A' A'' A' A''
6/m	\circ A_g	\circ \times A_g A_u	\circ \times \circ A_g A_u A_g	\circ \times \circ \times A_g A_u A_g A_u	\circ \times \circ \times \circ A_g A_u A_g A_u A_g	\circ \times \circ \times \circ \times A_g A_u A_g A_u A_g A_u
622	\circ A_1	\circ \times A_1 A_2	\circ \times \circ A_1 A_2 A_1	\circ \times \circ \times A_1 A_2 A_1 A_2	\circ \times \circ \times \circ A_1 A_2 A_1 A_2 A_1	\circ \times \circ \times \circ \times A_1 A_2 A_1 A_2 A_1 A_2
6mmm	\otimes A_1	\otimes \otimes \otimes A_1 A_1 A_1	\otimes \otimes \otimes A_1 A_1 A_1	\otimes \otimes \otimes \otimes A_1 A_1 A_1 A_1	\otimes \otimes \otimes \otimes \otimes A_1 A_1 A_1 A_1 A_1	\otimes \otimes \otimes \otimes \otimes \otimes A_1 A_1 A_1 A_1 A_1 A_1
$\bar{6}m2$	\circ A'_1	\circ \times A'_1 A'_2	\circ \times \circ A'_1 A'_2 A'_1	\circ \times \circ \times A'_1 A'_2 A'_1 A'_2	\circ \times \circ \times \circ A'_1 A'_2 A'_1 A'_2 A'_1	\circ \times \circ \times \circ \times A'_1 A'_2 A'_1 A'_2 A'_1 A'_2
6/mmm	\circ A_{1g}	\circ \times A_{1g} A_{2u}	\circ \times \circ A_{1g} A_{2u} A_{1g}	\circ \times \circ \times A_{1g} A_{2u} A_{1g} A_{2u}	\circ \times \circ \times \circ A_{1g} A_{2u} A_{1g} A_{2u} A_{1g}	\circ \times \circ \times \circ \times A_{1g} A_{2u} A_{1g} A_{2u} A_{1g} A_{2u}

TABLE V: C modes classification for a N -layer ML according to its point group G_N . For a given point group and N , the modes are reported from left to right in order of increasing frequency. Raman active modes are denoted as \circ , IR active ones as \times , while those that are both Raman and IR active as \otimes . A red symbol indicates that the Raman mode can be detected in a backscattering Raman experiment orthogonal to the layers. The irreducible representation to which each mode belongs is also reported. Whenever necessary, different orientations of the principal symmetry element with respect to the layering direction (z) are considered and specified in parenthesis. In cases where it is not possible to decouple C and LB modes, we still report them, and we note that the mode assignment coincides with that of the corresponding mixed mode in Table IV. Only modes along the first principal direction are reported if the pattern of Raman/IR activity is the same as for modes along second direction, and the irreducible representations differ just by a naming convention (e.g., B_2 vs B_3), otherwise displacements in both principal directions are shown.

Pointgroup	$N = 2$	$N = 3$	$N = 4$	$N = 5$	$N = 6$	$N = 7$
1	\otimes A	\otimes \otimes A A	\otimes \otimes \otimes A A A	\otimes \otimes \otimes \otimes A A A A	\otimes \otimes \otimes \otimes \otimes A A A A A	\otimes \otimes \otimes \otimes \otimes \otimes A A A A A A
$\bar{1}$	\circ A_g	\circ \times A_g A_u	\circ \times \circ A_g A_u A_g	\circ \times \circ \times A_g A_u A_g A_u	\circ \times \circ \times \circ A_g A_u A_g A_u A_g	\circ \times \circ \times \circ \times A_g A_u A_g A_u A_g A_u

Continues in the next page...

... continues from previous page.

Pointgroup	$N = 2$	$N = 3$	$N = 4$	$N = 5$	$N = 6$	$N = 7$
$\bar{3}m$	\circ E_g	$\circ \times$ $E_g E_u$	$\circ \times \circ$ $E_g E_u E_g$	$\circ \times \circ \times$ $E_g E_u E_g E_u$	$\circ \times \circ \times \circ$ $E_g E_u E_g E_u E_g$	$\circ \times \circ \times \circ \times$ $E_g E_u E_g E_u E_g E_u$
6	\otimes E_1	$\otimes \otimes$ $E_1 E_1$	$\otimes \otimes \otimes$ $E_1 E_1 E_1$	$\otimes \otimes \otimes \otimes$ $E_1 E_1 E_1 E_1$	$\otimes \otimes \otimes \otimes \otimes$ $E_1 E_1 E_1 E_1 E_1$	$\otimes \otimes \otimes \otimes \otimes \otimes$ $E_1 E_1 E_1 E_1 E_1 E_1$
$\bar{6}$	\circ E''	$\circ \otimes$ $E'' E'$	$\circ \otimes \circ$ $E'' E' E''$	$\circ \otimes \circ \otimes$ $E'' E' E'' E'$	$\circ \otimes \circ \otimes \circ$ $E'' E' E'' E' E''$	$\circ \otimes \circ \otimes \circ \otimes$ $E'' E' E'' E' E'' E'$
6/m	\circ E_{1g}	$\circ \times$ $E_{1g} E_{1u}$	$\circ \times \circ$ $E_{1g} E_{1u} E_{1g}$	$\circ \times \circ \times$ $E_{1g} E_{1u} E_{1g} E_{1u}$	$\circ \times \circ \times \circ$ $E_{1g} E_{1u} E_{1g} E_{1u} E_{1g}$	$\circ \times \circ \times \circ \times$ $E_{1g} E_{1u} E_{1g} E_{1u} E_{1g} E_{1u}$
622	\otimes E_1	$\otimes \otimes$ $E_1 E_1$	$\otimes \otimes \otimes$ $E_1 E_1 E_1$	$\otimes \otimes \otimes \otimes$ $E_1 E_1 E_1 E_1$	$\otimes \otimes \otimes \otimes \otimes$ $E_1 E_1 E_1 E_1 E_1$	$\otimes \otimes \otimes \otimes \otimes \otimes$ $E_1 E_1 E_1 E_1 E_1 E_1$
6mmm	\otimes E_1	$\otimes \otimes$ $E_1 E_1$	$\otimes \otimes \otimes$ $E_1 E_1 E_1$	$\otimes \otimes \otimes \otimes$ $E_1 E_1 E_1 E_1$	$\otimes \otimes \otimes \otimes \otimes$ $E_1 E_1 E_1 E_1 E_1$	$\otimes \otimes \otimes \otimes \otimes \otimes$ $E_1 E_1 E_1 E_1 E_1 E_1$
$\bar{6}m2$	\circ E''	$\circ \otimes$ $E'' E'$	$\circ \otimes \circ$ $E'' E' E''$	$\circ \otimes \circ \otimes$ $E'' E' E'' E'$	$\circ \otimes \circ \otimes \circ$ $E'' E' E'' E' E''$	$\circ \otimes \circ \otimes \circ \otimes$ $E'' E' E'' E' E'' E'$
6/mmm	\circ E_{1g}	$\circ \times$ $E_{1g} E_{1u}$	$\circ \times \circ$ $E_{1g} E_{1u} E_{1g}$	$\circ \times \circ \times$ $E_{1g} E_{1u} E_{1g} E_{1u}$	$\circ \times \circ \times \circ$ $E_{1g} E_{1u} E_{1g} E_{1u} E_{1g}$	$\circ \times \circ \times \circ \times$ $E_{1g} E_{1u} E_{1g} E_{1u} E_{1g} E_{1u}$

- [1] A. C. Ferrari, F. Bonaccorso, V. Fal'ko, K. S. Novoselov, S. Roche, P. Bøggild, S. Borini, F. H. L. Koppens, V. Palermo, N. Pugno, J. A. Garrido, R. Sordan, A. Bianco, L. Ballerini, M. Prato, E. Lidorikis, J. Kivioja, C. Marinelli, T. Ryhänen, A. Morpurgo, J. N. Coleman, V. Nicolosi, L. Colombo, A. Fert, M. Garcia-Hernandez, A. Bachtold, G. F. Schneider, F. Guinea, C. Dekker, M. Barbone, Z. Sun, C. Galiotis, A. N. Grigorenko, G. Konstantatos, A. Kis, M. Katsnelson, L. Vandersypen, A. Loiseau, V. Morandi, D. Neumaier, E. Treossi, V. Pellegrini, M. Polini, A. Tredicucci, G. M. Williams, B. Hee Hong, J.-H. Ahn, J. Min Kim, H. Zirath, B. J. van Wees, H. van der Zant, L. Occhipinti, A. Di Matteo, I. A. Kinloch, T. Seyller, E. Quesnel, X. Feng, K. Teo, N. Rupesinghe, P. Hakonen, S. R. T. Neil, Q. Tannock, T. Löfwander, and J. Kinaret, Science and technology roadmap for graphene, related two-dimensional crystals, and hybrid systems, *Nanoscale* **7**, 4598 (2015).
- [2] N. Mounet, M. Gibertini, P. Schwaller, D. Campi, A. Merkys, A. Marrazzo, T. Sohier, I. E. Castelli, A. Cepellotti, G. Pizzi, and N. Marzari, Two-dimensional materials from high-throughput computational exfoliation of experimentally known compounds, *Nature Nanotechnology* **13**, 246 (2018).
- [3] G. Cheon, K.-A. N. Duerloo, A. D. Sendek, C. Porter, Y. Chen, and E. J. Reed, Data Mining for New Two- and One-Dimensional Weakly Bonded Solids and Lattice-Commensurate Heterostructures, *Nano Letters* **17**, 1915 (2017).
- [4] M. Ashton, J. Paul, S. B. Sinnott, and R. G. Hennig, Topology-scaling identification of layered solids and stable exfoliated 2d materials, *Physical Review Letters* **118**, 106101 (2017).
- [5] K. Choudhary, I. Kalish, R. Beams, and F. Tavazza, High-throughput identification and characterization of two-dimensional materials using density functional theory, *Scientific Reports* **7**, 5179 (2017).
- [6] S. Haastруп, M. Strange, M. Pandey, T. Deilmann, P. S. Schmidt, N. F. Hinsche, M. N. Gjerding, D. Torelli, P. M. Larsen, A. C. Riis-Jensen, J. Gath, K. W. Jacobsen, J. J. Mortensen, T. Olsen, and K. S. Thygesen, The computational 2d materials database: high-throughput modeling and discovery of atomically thin crystals, *2D Materials* **5**, 042002 (2018).
- [7] J. Zhou, L. Shen, M. D. Costa, K. A. Persson, S. P. Ong, P. Huck, Y. Lu, X. Ma, Y. Chen, H. Tang, and Y. P. Feng, 2dmatpedia, an open computational database of two-dimensional materials from top-down and bottom-up approaches, *Scientific Data* **6**, 86 (2019).
- [8] C. Backes, A. M. Abdelkader, C. Alonso, A. Andrieux-Ledier, R. Arenal, J. Azpeitia, N. Balakrishnan, L. Banszerus, J. Barjon, R. Bartali, S. Bellani, C. Berger, R. Berger, M. M. B. Ortega, C. Bernard, P. H. Beton, A. Beyer, A. Bianco, P. Bøggild, F. Bonaccorso, G. B. Barin, C. Botas, R. A. Bueno, D. Carriazo, A. Castellanos-Gomez, M. Christian, A. Ciesielski, T. Ciuk, M. T. Cole, J. Coleman, C. Coletti, L. Crema, H. Cun, D. Dasler, D. D. Fazio, N. Díez, S. Drieschner, G. S. Duesberg, R. Fasel, X. Feng, A. Fina, S. Forti, C. Galiotis, G. Garberoglio, J. M. García, J. A. Garrido, M. Gibertini, A. Götzhäuser, J. Gómez, T. Greber, F. Hauke, A. Hemmi, I. Hernandez-Rodriguez, A. Hirsch, S. A. Hodge, Y. Huttel, P. U. Jepsen, I. Jimenez, U. Kaiser, T. Kaplas, H. Kim, A. Kis, K. Papagelis, K. Kostarelos, A. Krajewska, K. Lee, C. Li, H. Lipsaner, A. Liscio, M. R. Lohe, A. Loiseau, L. Lombardi, M. F. López, O. Martin, C. Martín, L. Martínez, J. A. Martin-Gago, J. I. Martínez, N. Marzari, Á. Mayoral, J. McManus, M. Melucci, J. Méndez, C. Merino, P. Merino, A. P. Meyer, E. Miniussi, V. Miseikis, N. Mishra,

- V. Morandi, C. Munuera, R. Muñoz, H. Nolan, L. Ortolani, A. K. Ott, I. Palacio, V. Palermo, J. Parthenios, I. Pasternak, A. Patane, M. Prato, H. Prevost, V. Prudkovskiy, N. Pugno, T. Rojo, A. Rossi, P. Ruffieux, P. Samori, L. Schué, E. Setijadi, T. Seyller, G. Speranza, C. Stampfer, I. Stenger, W. Strupinski, Y. Svirko, S. Taioli, K. B. K. Teo, M. Testi, F. Tomarchio, M. Tortello, E. Treossi, A. Turchanin, E. Vazquez, E. Vilaro, P. R. Whelan, Z. Xia, R. Yakimova, S. Yang, G. R. Yazdi, C. Yim, D. Yoon, X. Zhang, X. Zhuang, L. Colombo, A. C. Ferrari, and M. Garcia-Hernandez, Production and processing of graphene and related materials, *2D Materials* **7**, 022001 (2020).
- [9] A. Taghizadeh, U. Leffers, T. G. Pedersen, and K. S. Thygesen, A library of ab initio raman spectra for automated identification of 2d materials, *Nature Communications* **11**, 3011 (2020).
- [10] R. Bistritzer and A. H. MacDonald, Moiré bands in twisted double-layer graphene, *Proceedings of the National Academy of Sciences* **108**, 12233 (2011).
- [11] Y. Cao, V. Fatemi, A. Demir, S. Fang, S. L. Tomarken, J. Y. Luo, J. D. Sanchez-Yamagishi, K. Watanabe, T. Taniguchi, E. Kaxiras, R. C. Ashoori, and P. Jarillo-Herrero, Correlated insulator behaviour at half-filling in magic-angle graphene superlattices, *Nature* **556**, 80 (2018).
- [12] Y. Cao, V. Fatemi, S. Fang, K. Watanabe, T. Taniguchi, E. Kaxiras, and P. Jarillo-Herrero, Unconventional superconductivity in magic-angle graphene superlattices, *Nature* **556**, 43 (2018).
- [13] F. Wu, T. Lovorn, E. Tutuc, I. Martin, and A. H. MacDonald, Topological insulators in twisted transition metal dichalcogenide homobilayers, *Phys. Rev. Lett.* **122**, 086402 (2019).
- [14] H. Heo, J. H. Sung, S. Cha, B.-G. Jang, J.-Y. Kim, G. Jin, D. Lee, J.-H. Ahn, M.-J. Lee, J. H. Shim, H. Choi, and M.-H. Jo, Interlayer orientation-dependent light absorption and emission in monolayer semiconductor stacks, *Nature Communications* **6**, 7372 (2015).
- [15] P. K. Nayak, Y. Horbatenko, S. Ahn, G. Kim, J.-U. Lee, K. Y. Ma, A.-R. Jang, H. Lim, D. Kim, S. Ryu, H. Cheong, N. Park, and H. S. Shin, Probing evolution of twist-angle-dependent interlayer excitons in MoSe₂/WSe₂ van der Waals heterostructures, *ACS Nano* **11**, 4041 (2017), pMID: 28363013, <https://doi.org/10.1021/acsnano.7b00640>.
- [16] E. M. Alexeev, D. A. Ruiz-Tijerina, M. Danovich, M. J. Hamer, D. J. Terry, P. K. Nayak, S. Ahn, S. Pak, J. Lee, J. I. Sohn, M. R. Molas, M. Koperski, K. Watanabe, T. Taniguchi, K. S. Novoselov, R. V. Gorbachev, H. S. Shin, V. I. Fal'ko, and A. I. Tartakovskii, Resonantly hybridized excitons in Moiré superlattices in van der Waals heterostructures, *Nature* **567**, 81 (2019).
- [17] K. Tran, G. Moody, F. Wu, X. Lu, J. Choi, K. Kim, A. Rai, D. A. Sanchez, J. Quan, A. Singh, J. Embrey, A. Zepeda, M. Campbell, T. Autry, T. Taniguchi, K. Watanabe, N. Lu, S. K. Banerjee, K. L. Silverman, S. Kim, E. Tutuc, L. Yang, A. H. MacDonald, and X. Li, Evidence for Moiré excitons in van der Waals heterostructures, *Nature* **567**, 71 (2019).
- [18] K. L. Seyler, P. Rivera, H. Yu, N. P. Wilson, E. L. Ray, D. G. Mandrus, J. Yan, W. Yao, and X. Xu, Signatures of Moiré-trapped valley excitons in MoSe₂/WSe₂ heterobilayers, *Nature* **567**, 66 (2019).
- [19] C. Jin, E. C. Regan, A. Yan, M. Iqbal Bakti Utama, D. Wang, S. Zhao, Y. Qin, S. Yang, Z. Zheng, S. Shi, K. Watanabe, T. Taniguchi, S. Tongay, A. Zettl, and F. Wang, Observation of Moiré excitons in WSe₂/WS₂ heterostructure superlattices, *Nature* **567**, 76 (2019).
- [20] C. Casiraghi, A. Hartschuh, E. Lidorikis, H. Qian, H. Harutyunyan, T. Gokus, K. S. Novoselov, and A. C. Ferrari, Rayleigh imaging of graphene and graphene layers, *Nano Letters*, *Nano Letters* **7**, 2711 (2007).
- [21] A. C. Ferrari and D. M. Basko, Raman spectroscopy as a versatile tool for studying the properties of graphene, *Nature Nanotechnology* **8**, 235 (2013).
- [22] J.-W. Jiang, H. Tang, B.-S. Wang, and Z.-B. Su, Raman and infrared properties and layer dependence of the phonon dispersions in multilayered graphene, *Phys. Rev. B* **77**, 235421 (2008).
- [23] J. Ji, S. Dong, A. Zhang, and Q. Zhang, Low-frequency interlayer vibration modes in two-dimensional layered materials, *Physica E: Low-dimensional Systems and Nanostructures* **80**, 130 (2016).
- [24] X. Zhang, Q.-H. Tan, J.-B. Wu, W. Shi, and P.-H. Tan, Review on the Raman spectroscopy of different types of layered materials, *Nanoscale* **8**, 6435 (2016).
- [25] L. Liang, J. Zhang, B. G. Sumpter, Q.-H. Tan, P.-H. Tan, and V. Meunier, Low-frequency shear and layer-breathing modes in Raman scattering of two-dimensional materials, *ACS Nano*, *ACS Nano* **11**, 11777 (2017).
- [26] P. H. Tan, W. P. Han, W. J. Zhao, Z. H. Wu, K. Chang, H. Wang, Y. F. Wang, N. Bonini, N. Marzari, N. Pugno, G. Savini, A. Lombardo, and A. C. Ferrari, The shear mode of multilayer graphene, *Nature Mater.* **11**, 294 (2012).
- [27] C. H. Lui, L. M. Malard, S. Kim, G. Lantz, F. E. Laverge, R. Saito, and T. F. Heinz, Observation of layer-breathing mode vibrations in few-layer graphene through combination Raman scattering, *Nano Letters*, *Nano Letters* **12**, 5539 (2012).
- [28] J.-B. Wu, X. Zhang, M. Ijäs, W.-P. Han, X.-F. Qiao, X.-L. Li, D.-S. Jiang, A. C. Ferrari, and P.-H. Tan, Resonant Raman spectroscopy of twisted multilayer graphene, *Nature Commu.* **5**, 5309 (2014).
- [29] J.-B. Wu, Z.-X. Hu, X. Zhang, W.-P. Han, Y. Lu, W. Shi, X.-F. Qiao, M. Ijäs, S. Milana, W. Ji, A. C. Ferrari, and P.-H. Tan, Interface coupling in twisted multilayer graphene by resonant Raman spectroscopy of layer breathing modes, *ACS Nano*, *ACS Nano* **9**, 7440 (2015).
- [30] X. Zhang, W. P. Han, J. B. Wu, S. Milana, Y. Lu, Q. Q. Li, A. C. Ferrari, and P. H. Tan, Raman spectroscopy of shear and layer breathing modes in multilayer MoS₂, *Phys. Rev. B* **87**, 115413 (2013).
- [31] M. Boukhicha, M. Calandra, M.-A. Measson, O. Lancry, and A. Shukla, Anharmonic phonons in few-layer MoS₂: Raman spectroscopy of ultralow energy compression and shear modes, *Phys. Rev. B* **87**, 195316 (2013).
- [32] K. Kim, J.-U. Lee, D. Nam, and H. Cheong, Davydov splitting and excitonic resonance effects in Raman spectra of few-layer MoSe₂, *ACS Nano*, *ACS Nano* **10**, 8113 (2016).
- [33] J. Yang, J.-U. Lee, and H. Cheong, Excitation energy dependence of Raman spectra of few-layer WS₂, *FlatChem* **3**, 64 (2017).
- [34] Y. Zhao, X. Luo, H. Li, J. Zhang, P. T. Araujo, C. K. Gan, J. Wu, H. Zhang, S. Y. Quek, M. S. Dresselhaus, and Q. Xiong, Interlayer breathing and shear modes in

- few-trilayer MoS₂ and WSe₂, *Nano Lett.* **13**, 1007 (2013), <http://dx.doi.org/10.1021/nl304169w>.
- [35] Q. J. Song, Q. H. Tan, X. Zhang, J. B. Wu, B. W. Sheng, Y. Wan, X. Q. Wang, L. Dai, and P. H. Tan, Physical origin of davydov splitting and resonant Raman spectroscopy of Davydov components in multilayer MoTe₂, *Phys. Rev. B* **93**, 115409 (2016).
- [36] G. Froehlicher, E. Lorchat, F. Fernique, C. Joshi, A. Molina-Sánchez, L. Wirtz, and S. Berciaud, Unified description of the optical phonon modes in N-layer MoTe₂, *Nano Lett.* **15**, 6481 (2015), <http://dx.doi.org/10.1021/acs.nanolett.5b02683>.
- [37] P. Nagler, G. Plechinger, C. Schüller, and T. Korn, Observation of anisotropic interlayer Raman modes in few-layer ReS₂, *Phys. Status Solidi Rapid Res. Lett.* **10.1002/pssr.201510412** (2015).
- [38] H. Zhao, J. Wu, H. Zhong, Q. Guo, X. Wang, F. Xia, L. Yang, P. Tan, and H. Wang, Interlayer interactions in anisotropic atomically thin rhenium diselenide, *Nano Research* **8**, 3651 (2015).
- [39] X.-F. Qiao, J.-B. Wu, L. Zhou, J. Qiao, W. Shi, T. Chen, X. Zhang, J. Zhang, W. Ji, and P.-H. Tan, Polytypism and unexpected strong interlayer coupling in two-dimensional layered ReS₂, *Nanoscale* **8**, 8324 (2016).
- [40] Y. Zhao, J. Qiao, P. Yu, Z. Hu, Z. Lin, S. P. Lau, Z. Liu, W. Ji, and Y. Chai, Extraordinarily strong interlayer interaction in 2D layered PtS₂, *Advanced Materials* **28**, 2399 (2016).
- [41] X. Xi, L. Zhao, Z. Wang, H. Berger, L. Forró, J. Shan, and K. F. Mak, Strongly enhanced charge-density-wave order in monolayer NbSe₂, *Nature Nanotechnology* **10**, 765 (2015).
- [42] R. He, J. van Baren, J.-A. Yan, X. Xi, Z. Ye, G. Ye, L.-H. Lu, S. M. Leong, and C. H. Lui, Interlayer breathing and shear modes in NbSe₂ atomic layers, *2D Materials* **3**, 031008 (2016).
- [43] G. J. Orchin, D. De Fazio, A. Di Bernardo, M. Hamer, D. Yoon, A. R. Cadore, I. Goykhman, K. Watanabe, T. Taniguchi, J. W. A. Robinson, R. V. Gorbachev, A. C. Ferrari, and R. H. Hadfield, Niobium diselenide superconducting photodetectors, *Applied Physics Letters* **114**, 251103 (2019).
- [44] I. Stenger, L. Schué, M. Boukhicha, B. Berini, B. Plaças, A. Loiseau, and J. Barjon, Low frequency raman spectroscopy of few-atomic-layer thick hBN crystals, *2D Materials* **4**, 031003 (2017).
- [45] X. Ling, L. Liang, S. Huang, A. A. Puretzky, D. B. Gehegan, B. G. Sumpter, J. Kong, V. Meunier, and M. S. Dresselhaus, Low-frequency interlayer breathing modes in few-layer black phosphorus, *Nano Letters* **15**, 4080 (2015).
- [46] X. Luo, X. Lu, G. K. W. Koon, A. H. C. Neto, B. Özyilmaz, Q. Xiong, and S. Y. Quek, Large frequency change with thickness in interlayer breathing mode—significant interlayer interactions in few layer black phosphorus, *Nano Lett.* **15**, 3931 (2015).
- [47] S. Dong, A. Zhang, K. Liu, J. Ji, Y. G. Ye, X. G. Luo, X. H. Chen, X. Ma, Y. Jie, C. Chen, X. Wang, and Q. Zhang, Ultralow-frequency collective compression mode and strong interlayer coupling in multilayer black phosphorus, *Phys. Rev. Lett.* **116**, 087401 (2016).
- [48] Y. Zhao, X. Luo, J. Zhang, J. Wu, X. Bai, M. Wang, J. Jia, H. Peng, Z. Liu, S. Y. Quek, and Q. Xiong, Interlayer vibrational modes in few-quintuple-layer Bi₂Te₃ and Bi₂Se₃ two-dimensional crystals: Raman spectroscopy and first-principles studies, *Phys. Rev. B* **90**, 245428 (2014).
- [49] S. Y. Lim, J.-U. Lee, J. H. Kim, L. Liang, X. Kong, T. T. H. Nguyen, Z. Lee, S. Cho, and H. Cheong, Polytypism in few-layer gallium selenide, *Nanoscale* **12**, 8563 (2020).
- [50] M. R. Molas, A. Tyurnina, V. Zolyomi, A. Ott, D. J. Terry, M. Hamer, C. Yegel, A. Babiński, A. G. Nasibulin, A. C. Ferrari, V. Fal’ko, and R. Gorbachev, Raman spectroscopy of gase and inse post-transition metal chalcogenides layers, *Faraday Discussions*, (2020), <http://doi.org/10.1039/D0FD00007H>.
- [51] T. Sriv, K. Kim, and H. Cheong, Low-frequency raman spectroscopy of few-layer 2H-SnS₂, *Scientific Reports* **8**, 10194 (2018).
- [52] L. Talirz, S. Kumbhar, E. Passaro, A. V. Yakutovich, V. Granata, F. Gargiulo, M. Borelli, M. Uhrin, S. P. Huber, S. Zoupanos, C. S. Adorf, C. W. Andersen, O. Schütt, C. A. Pignedoli, D. Passerone, J. VandeVondele, T. C. Schulthess, B. Smit, G. Pizzi, and N. Marzari, Materials Cloud, a platform for open computational science, *Scientific Data* **7**, 299 (2020).
- [53] A. C. Ferrari, J. C. Meyer, V. Scardaci, C. Casiraghi, M. Lazzeri, F. Mauri, S. Piscanec, D. Jiang, K. S. Novoselov, S. Roth, and A. K. Geim, Raman spectrum of graphene and graphene layers, *Phys. Rev. Lett.* **97**, 187401 (2006).
- [54] S. Đurovič, P. Krishna, and D. Pandey, Layer stacking, in *International Tables for Crystallography Volume C: Mathematical, physical and chemical tables*, edited by E. Prince (Springer Netherlands, Dordrecht, 2006) pp. 752–773.
- [55] A. Guinier, G. B. Bokij, K. Boll-Dornberger, J. M. Cowley, S. Đurovič, H. Jagodzinski, P. Krishna, P. M. de Wolff, B. B. Zvyagin, D. E. Cox, P. Goodman, T. Hahn, K. Kuchitsu, and S. C. Abrahams, Nomenclature of polytype structures. Report of the International Union of Crystallography *Ad hoc* Committee on the Nomenclature of Disordered, Modulated and Polytype Structures, *Acta Crystallographica Section A* **40**, 399 (1984).
- [56] K. Dornberger-Schiff, *Grundzüge einer Theorie der OD-Strukturen aus Schichten*, Abhandlungen der Deutschen Akademie der Wissenschaften zu Berlin, Klasse für Chemie, Geologie und Biologie (Akad.-Verl., Berlin, 1964) p. 106pp.
- [57] K. Dornberger-Schiff and K. Fichtner, On the Symmetry of OD-Structures Consisting of Equivalent Layers, *Kristall und Technik* **7**, 1035 (1972).
- [58] A. J. Molina-Mendoza, E. Giovanelli, W. S. Paz, M. A. Niño, J. O. Island, C. Evangelini, L. Aballe, M. Foerster, H. S. J. van der Zant, G. Rubio-Bollinger, N. Agrait, J. J. Palacios, E. M. Pérez, and A. Castellanos-Gomez, Franckeite as a naturally occurring van der waals heterostructure, *Nature Communications* **8**, 14409 (2017).
- [59] M. Velický, P. S. Toth, A. M. Rakowski, A. P. Rooney, A. Kozikov, C. R. Woods, A. Mishchenko, L. Fumagalli, J. Yin, V. Zolyomi, T. Georgiou, S. J. Haigh, K. S. Novoselov, and R. A. W. Dryfe, Exfoliation of natural van der Waals heterostructures to a single unit cell thickness, *Nature Communications* **8**, 14410 (2017).
- [60] S. Gražulis, A. Daškevič, A. Merkys, D. Chateigner,

- L. Lutterotti, M. Quirós, N. R. Serebryanaya, P. Moeck, R. T. Downs, and A. Le Bail, Crystallography open database (COD): an open-access collection of crystal structures and platform for world-wide collaboration, *Nucleic Acids Research* **40**, D420 (2012).
- [61] A. Belsky, M. Hellenbrandt, V. L. Karen, and P. Luksch, New developments in the Inorganic Crystal Structure Database (ICSD): accessibility in support of materials research and design, *Acta Crystallographica Section B* **58**, 364 (2002).
- [62] N. Scheuschner, R. Gillen, M. Staiger, and J. Maultzsch, Interlayer resonant Raman modes in few-layer MoS₂, *Phys. Rev. B* **91**, 235409 (2015).
- [63] M. O’Keeffe and B. Hyde, *Crystal Structures I. Patterns and Symmetry* (Mineralogical Society of America, 1996).
- [64] B. Souvignier, H. Wondratschek, M. I. Aroyo, G. Chapuis, and A. M. Glazer, Space groups and their descriptions, in *International Tables for Crystallography Volume A* (International Union of Crystallography, 2016) pp. 42–74.
- [65] U. Shmueli, S. R. Hall, and R. W. Grosse-Kunstleve, Symmetry in reciprocal space, in *International Tables for Crystallography Volume B* (International Union of Crystallography, 2010) pp. 114–174.
- [66] S. R. Hall, Space-group notation with an explicit origin, *Acta Crystallographica Section A* **37**, 517 (1981).
- [67] T. Wieting, Long-wavelength lattice vibrations of MoS₂ and GaSe, *Solid State Communications* **12**, 931 (1973).
- [68] J. Nye, *Physical properties of crystals: Their representation by tensor and matrices* (Oxford University Press, 1957).
- [69] C. Bradley and A. Cracknell, *The Mathematical Theory of Symmetry in Solids: Representation Theory for Point Groups and Space Groups* (Oxford University Press, Oxford, 2010).
- [70] S. Altmann and P. Herzig, *Point-group Theory Tables*, Oxford science publications (Clarendon Press, 1994).
- [71] M. Aroyo, J. Perez-Mato, D. Orobengoa, E. Tasci, G. De La Flor, and A. Kirov, Crystallography online: Bilbao crystallographic server, *Bulgarian Chemical Communications* **43**, 183 (2011).
- [72] M. Dresselhaus, G. Dresselhaus, and A. Jorio, *Group Theory. Application to the Physics of Condensed Matter* (Springer-Verlag, 2008).
- [73] H. R. Hoekstra, S. Siegel, and F. X. Gallagher, Reaction of platinum dioxide with some metal oxides, in *Platinum Group Metals and Compounds*, Vol. 98, edited by U. V. Rao (American Chemical Society, 1971) Chap. 4, pp. 39–53.
- [74] A. H. Larsen, J. J. Mortensen, J. Blomqvist, I. E. Castelli, R. Christensen, M. Dułak, J. Friis, M. N. Groves, B. Hammer, C. Hargus, E. D. Hermes, P. C. Jennings, P. B. Jensen, J. Kermode, J. R. Kitchin, E. L. Kolsbjerg, J. Kubal, K. Kaasbjerg, S. Lysgaard, J. B. Maronsson, T. Maxson, T. Olsen, L. Pastewka, A. Peterson, C. Rostgaard, J. Schiøtz, O. Schütt, M. Strange, K. S. Thygesen, T. Vegge, L. Vilhelmsen, M. Walter, Z. Zeng, and K. W. Jacobsen, The atomic simulation environment—a python library for working with atoms, *Journal of Physics: Condensed Matter* **29**, 273002 (2017).
- [75] S. P. Ong, W. D. Richards, A. Jain, G. Hautier, M. Kocher, S. Cholia, D. Gunter, V. L. Chevrier, K. A. Persson, and G. Ceder, Python materials genomics (pymatgen): A robust, open-source python library for materials analysis, *Computational Materials Science* **68**, 314 (2013).
- [76] B. Cordero, V. Gómez, A. E. Platero-Prats, M. Revés, J. Echeverría, E. Cremades, F. Barragán, and S. Alvarez, Covalent radii revisited, *Dalton Trans.* , 2832 (2008).